RESEARCH ARTICLE | MAY 23 2024

Deep cavity noise suppression by exploiting aeroacoustic–structural interaction of multiple elastic panels

Muhammad Rehan Naseer ; Irsalan Arif ; Randolph C. K. Leung ; Ali Abdullah

Physics of Fluids 36, 057141 (2024)
https://doi.org/10.1063/5.0206185

Physics of Fluids ARTICLE pubs.aip.org/aip/pof

Deep cavity noise suppression by exploiting aeroacoustic–structural interaction of multiple elastic panels

Cite as: Phys. Fluids **36**, 057141 (2024); doi: 10.1063/5.0206185
Submitted: 29 February 2024 · Accepted: 1 May 2024 ·
Published Online: 23 May 2024

Muhammad Rehan Naseer,[1] Irsalan Arif,[2] Randolph C. K. Leung,[1,a)] and Ali Abdullah[1]

AFFILIATIONS

[1]Department of Mechanical Engineering, The Hong Kong Polytechnic University, Hong Kong, People's Republic of China
[2]College of Aeronautical Engineering, National University of Sciences and Technology, Islamabad, Pakistan

[a)]Author to whom correspondence should be addressed: mmrleung@polyu.edu.hk

ABSTRACT

This paper reports a numerical study of a novel methodology for passive suppression of deep cavity noise by means of strategically designed and arrangements of multiple elastic panels and examines its underlying aeroacoustic–structural interaction physics. The study is conducted with a freestream, at Mach number 0.09 and Reynolds number of 4×10^4 based on the cavity length, past a two-dimensional cavity by means of direct aeroacoustic simulation coupled with a panel dynamic solver in monolithic fashion. For each cavity-panel configuration, the fluid-loaded panel natural frequencies are harmonized with the characteristic aeroacoustic processes of the original/modified cavity aeroacoustic feedback loop. This promotes panel aeroacoustic-structural resonance for absorption of feedback flow and acoustic fluctuation energy for achieving less eventual cavity noise. The most effective configuration gives a remarkable noise power reduction by 15 dB from a rigid cavity. Inadvertently, it reduces cavity drag by almost 15%. Simultaneous reduction of both cavity noise and drag is unprecedented among similar attempts in the literature. In-depth spatiotemporal analyses of aeroacoustic–structural interaction results elucidate the intricate interplay between cavity flow, panel vibration responses, and cavity acoustic modes, leading to noise reduction in all cavity-panel configurations studied. Essentially, the vertical panel acts to curtail the efficacy of coupling between growing shear layer and cavity acoustic modes whose sustenance is further impeded by an acoustically induced resonant panel at the cavity bottom. The proposed methodology is confirmed to be feasible yet effective, which holds great potential for fluid-moving applications in which a quiet and energy-efficient cavity configuration is desired.

I. INTRODUCTION

The flow over a rectangular cavity has garnered significant research interest over the past few decades due to its prevalent occurrence in various real-world engineering applications. Under a certain range of operating conditions, the unsteady flow over the cavity may excite a self-sustained oscillation that would couple with a cavity acoustic mode to generate intense flow-induced noise. This noise is a concern in various contexts, notably in high-speed aeronautical flows through open cavities like weapon bays and wheel wells, where it causes density and pressure fluctuations, increased sound levels, and intense vibrations. Such issues are particularly challenging in military aircraft during store deployment (Liu *et al.*, 2024; Cattafesta III *et al.*, 2008). In a railway, aerodynamic noise from train car and bogie gaps escalates with train speed (He *et al.*, 2024; Talotte, 2000), necessitating effective noise reduction methods. Similarly, the automotive industry grapples with sunroof buffeting (Kook *et al.*, 1997), causing increased interior noise and passenger discomfort. In gas transportation, cavity flow phenomena are akin to aeroacoustic pulsations from flow instabilities in closed branches, potentially leading to pre-mature mechanical failures due to high amplitude acoustic pressure fluctuations (Wang *et al.*, 2024; Bruggeman *et al.*, 1991; and Ziada, 2010). Turbomachinery also experiences related challenges, where impinging shear layers cause unsteady pressure loading and noise radiation (Rebholz *et al.*, 2016; Ziada *et al.*, 2002). These flow-induced oscillations, primarily hydrodynamic, may interact with resonant acoustic modes in cavities, risking structural failures in engine components. This complexity across applications underscores the need for a better understanding of acoustic and vortical fluctuations and managing multiple cavity resonant modes for effective suppression of oscillations. Flow-induced cavity oscillations, thus, represent a canonical control problem in fluid mechanics and aeroacoustics, requiring focused research and innovative solutions. This study aims to contribute to the understanding and

mitigation of cavity flow-induced oscillations leading to the extreme noise radiation.

Plentovich *et al.* (1993) conducted an extensive experimental investigation into cavity flow at low to high subsonic freestream Mach numbers ($0.2 \leq M \leq 0.95$) and a broad range of Reynolds numbers ($0.2–18 \times 10^6$) based on cavity length. They categorized the cavity flow into open, closed, and transitional types and identified the limits of cavity dimensions, specifically the length-to-depth ratio (L/D), for delineating different flow responses. For open cavity flow ($L/D \lesssim 8$), the shear layer extends across the cavity opening and its impact at the cavity trailing edge generates tonal noise. Conversely, in closed cavity flows ($L/D \gtrsim 13$), the inflow separates at the leading edge but lacks the energy to cross the cavity, reattaching to the cavity floor before reaching the trailing edge, without producing a significant acoustic signature. Transitional cavity flow, with dimensions within $8 \lesssim L/D \lesssim 13$, displays characteristics of both open and closed types.

A key aspect of open cavity flow is the strong tonal noise radiation at discrete frequencies across a broad frequency range. Noise radiation characteristics differ between shallow ($L/D > 1$) and deep cavity configurations ($L/D < 1$). This differentiation was initially observed by Covert (1970) and further highlighted by Heller and Bliss (1975), who noted distinct patterns of aeroacoustic coupling in deep cavities compared to shallow ones. Later, Rockwell and Naudascher (1978) recognized the unique flow responses in both shallow and deep open cavities as a canonical type of fluid-resonant oscillation. They identified this based on the observed acoustic reinforcement of shear layer instabilities at the cavity leading edge, which closes the feedback loop for self-sustained resonant flow oscillations, regardless of whether the cavity operates in transverse or longitudinal acoustic modes depending on its dimensions.

Rossiter (1964) introduced a theoretical framework for the self-sustaining oscillations observed in shallow cavity flows and provided an empirical formula to predict their dominant frequencies. His model elucidates the feedback loop essential for tonal noise production when a grazing flow interacts with a shallow cavity. This process is initiated by Kelvin–Helmholtz instabilities in the shear layer, which intensify as they propagate downstream. The impingement of these amplified instabilities on the cavity trailing edge generates acoustic waves that travel upstream to reinforce further instabilities in the shear layer. The validity and prevalence of the Rossiter model have been supported and extended by subsequent experimental and numerical studies (Arya and De, 2021; Liu and Gaitonde, 2021).

For deep cavities, extensive studies (East, 1966; Ziada and Bühlmann, 1992; and Ho and Kim, 2021) indicate that the oscillations of the shear layer at the cavity opening activate the acoustic modes within the cavity depth and the synergistic interaction between the flow dynamics and acoustic modes results in noise radiation from deep cavities. While deep cavities operate differently from shallow ones, the Rossiter formula, with appropriate adjustments, remains effective in forecasting the oscillation frequencies within the deep cavity flow field (Heller and Bliss, 1975). In particular, at flow frequencies that align closely with the cavity natural modes, deep cavities set in maximal acoustic resonance (East, 1966; Ho and Kim, 2021), emphasizing the intricate relationship between flow dynamics and acoustic responses in cavity flows. Bruggeman *et al.* (1989) proposed an alternate feedback mechanism for fluid-resonant oscillations, withholding the principles of vortex sound theory (Howe, 2002). The mechanism encompasses a series of interrelated processes: namely, the resonant acoustic excitation of the shear layer emanating from the cavity leading edge; the formation of coherent vortices due to instabilities in the separated shear layer; the transfer of energy from the local flow to the acoustic field facilitated by the interaction between convective vorticity and acoustic resonance; and the resultant net energy contribution to the cavity acoustic field. The energy transfer may destabilize the shear layer growth and augment vortex coalescence, contingent upon specific amplitudes and phases of the feedback loop at the cavity leading edge. This theoretical framework provides a plausible explanation for the lock-on effect frequently observed in experimental investigations of deep cavities, as evidenced by studies conducted by (Yang *et al.*, 2009; Yokoyama *et al.*, 2016; and Ho and Kim, 2021). The depth of insight offered by the model of Bruggeman *et al.* (1989) significantly enhances our understanding of the complex interactions underpinning fluid-resonant oscillations in cavity flows.

In an attempt to further elucidate the aeroacoustic driving mechanism in deep cavities, Naseer *et al.* (2023) have revealed that the aeroacoustic feedback process in deep cavities consists of five distinct processes, each of which is supported by the corresponding cavity walls. First, the boundary layer develops at the upstream cavity wall. Upon separating from the cavity leading edge, and with acoustic reinforcement by the reflected acoustic mode supported by the cavity front wall, the shear layer emanates and evolves over the cavity opening. Second, vortices of a fully developed shear layer reach the cavity trailing edge, where vortex impingement occurs, supported by the cavity aft wall. Third, the residual eclipsed shear layer vortices convect over the downstream wall. Afterwards, the high strain impingement of the shear layer at the aft wall produces strong pressure waves directed toward the cavity bottom. Eventually, these waves are then reflected back, reinforcing the developing shear layer and closing the feedback loop. Recent studies have also provided insights into the mechanisms of cavity flow-induced noise. Liu *et al.* (2023) investigated Rossiter resonance noise in a low-speed wind tunnel, highlighting the interaction between Rossiter modes and depth resonant modes in locked-on states, offering a modified Rossiter formula that considers phase delay variations with velocity for more accurate predictions. Similarly, Wang *et al.* (2024) explored the interplay of flow and acoustics within tandem deep cavities, focusing on the resonance mechanism between turbulent shear layers and acoustic eigenmodes, advancing our understanding of aeroacoustic interactions in complex cavity configurations.

Over the recent years, a variety of passive and active techniques aimed at altering the flow dynamics at the leading or trailing edges [Fig. 1(a)] of cavities have been explored to attenuate their Rossiter modes, thereby reducing cavity noise (Lee, 2010; Liu and Gómez, 2019; Saddington *et al.*, 2016; Li *et al.*, 2020; Abdelmwgoud and Mohany, 2021; and Mourão Bento *et al.*, 2022). A noteworthy passive approach includes the use of micro-perforated panels, which Maury *et al.* (2019) demonstrated could reduce cavity pressure fluctuations by up to 8 dB in transitional cavity flow regimes, showcasing their effectiveness without altering the fundamental flow characteristics. Yokoyama *et al.* (2020) endeavored to enhance the efficiency of actuation energy in cavity noise reduction by substituting flow jets with continuous and intermittent plasma actuators at the leading edge. Their results demonstrated that considerable noise reduction is achievable with reduced, though still substantial, actuation power input, plateauing with further power increases. Additionally, recent numerical

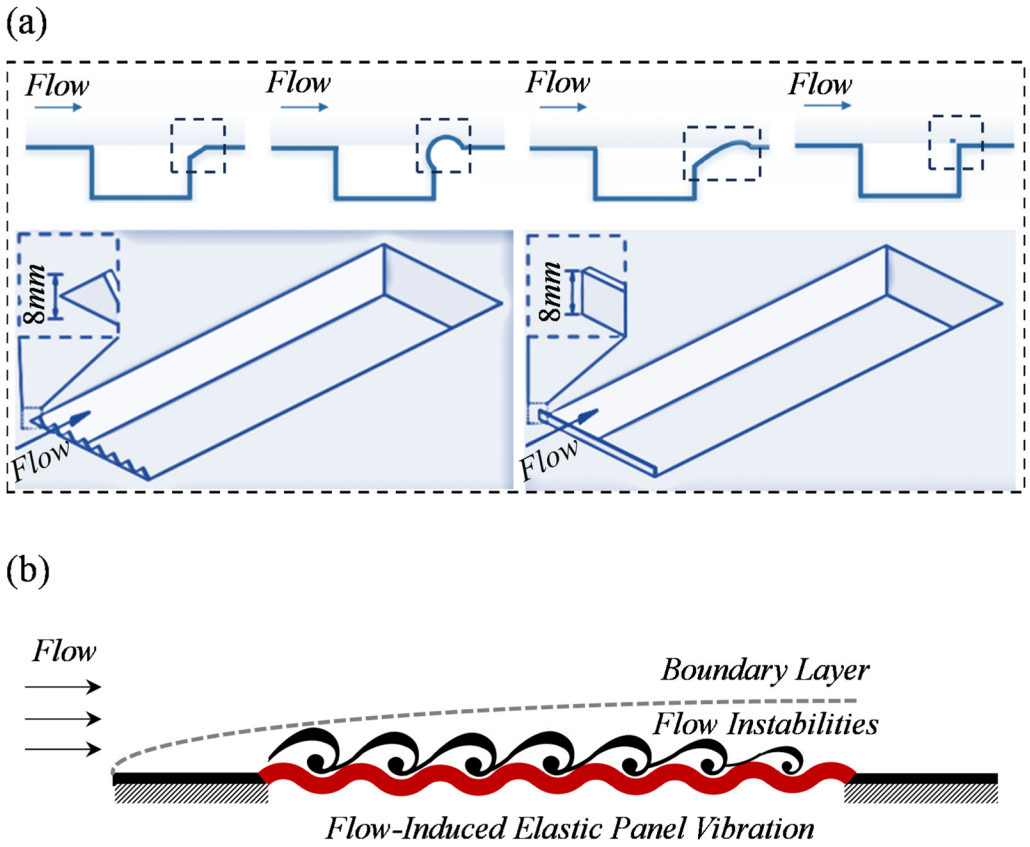

FIG. 1. (a) Traditional cavity noise reduction techniques. [Reproduced with permission from Liu and Gómez, AIAA J. **57**(2), 876–878 (2019). Copyright 2019 Author(s). Reproduced with permission from Saddington *et al.*, J. Aircraft **53**(5), 1439–1447 (2016). Copyright 2016 Author(s).] (b) The novel cavity noise suppression concept proposed in the present study.

studies by Bacci and Saddington (2023) highlighted the impact of structural modifications, such as introducing a gap between the doors and the cavity edge on a weapon bay model, which showed a strong palliative effect on the aeroacoustic and structural response, including a notable fluid–acoustic coupling at the first structural mode frequency. Furthermore, Bacci and Saddington (2022) conducted Hilbert–Huang spectral analysis on cavities with fluidic spoilers, revealing that these spoilers significantly mitigate acoustic noise and modify shear layer trajectories, thus altering resonant modes and their interaction with Rossiter–Heller tones in a complex nonlinear manner. It is important to note that these noise suppression methods are intrinsically flow-invasive. Their implementation invariably introduces substantial disturbances to the evolving cavity shear layer, thereby altering the fundamental flow characteristics inherent to the original cavity configuration. This may lead to a range of unintended aerodynamic effects, such as intensified turbulence, increased flow-induced drag, and elevated actuation energy requirements as a result of the traditional treatment for cavity noise reduction. Moreover, these methods may induce extraneous noise in frequency ranges absent in the original flow. Unfortunately, these potential drawbacks have not been comprehensively addressed in the existing literature.

The present study introduces and examines a novel passive approach for mitigating noise radiation by deep cavities, employing a localized surface compliance [Fig. 1(b)] mechanism realized through an arrangement of strategically designed multiple elastic panels. Each panel in this arrangement is tailored to target a certain constituent process of the deep cavity aeroacoustic mechanism. With the synergistic action of its flow-induced panel vibration, every panel is expected to maximize noise reduction potential. The underlying principle of the proposed approach is to harness flow-induced panel resonant vibrations, which are set to absorb flow energy to alter or decouple the aeroacoustic feedback mechanisms driving the fluid-resonant oscillations inside the deep cavity. The proposed approach has two primary advantages. First, the vibratory displacement of each resonant panel is deliberately kept smaller than the typical dimensions of the cavity, thus minimizing distortion of streamlines around the panel. Second, the panels, in a state of structural resonance, function to absorb flow fluctuation energy through a reactive mechanism rather than a dissipative one, which gives the potential to leave cavity drag unaffected. This approach is, thus, expected to reduce cavity noise while maintaining the cavity intrinsic flow characteristics.

To explore the spatiotemporal aeroacoustic–structural interaction between the cavity flow field and the vibrating elastic panels, this study utilizes an in-house Direct Aeroacoustics Simulation (DAS) code solved with the conservation element and solution element (CE/SE) method. This is supplemented by extensive analyses focused on panel

design, cavity noise reduction, and panel dynamics. The panels are intricately designed to resonate with the imparted flow for effective absorption of flow fluctuation energy. Strategic placement of the panels within the cavity targets to weaken the various aeroacoustic feedback and coupling processes, thereby mitigating fluid resonant cavity oscillations. This paper presents a comprehensive aeroacoustic–structural interaction analysis to ascertain the effectiveness of our proposed noise suppression approach and thoroughly examines its modification of cavity flow characteristics. Furthermore, the study delves into an analysis of the flow dynamic consequences resulting from this control method. Understanding these consequences is vital for assessing the practicality of the proposed approach in real-world engineering applications, an aspect frequently overlooked in the existing literature of similar problems.

The structure of this paper is laid out as follows: Sec. II delves into the problem formulation and the numerical methods utilized in this study. In Sec. III, we detail the comprehensive design methodology for cavity-panel configurations, focusing on single-panel arrangements. The insights gained from this analysis provide the foundation for the design of multiple panel configurations, which are thoroughly explored in Sec. IV. Section V is dedicated to examining the impact of flow-induced panel vibrations on the development of deep cavity aeroacoustics. Section VI deals with an in-depth study of the mechanisms underlying cavity noise suppression. Finally, Sec. VII investigates the roles of aeroacoustic–structural responses of elastic panels in various configurations, specifically in relation to their effectiveness in suppressing cavity noise.

II. NUMERICAL METHODOLOGY AND COMPUTATIONAL SETUP

We utilized a Direct Aeroacoustics Simulation (DAS) approach and the robust Conservation Element and Solution Element (CE/SE) method to address the normalized compressible Navier–Stokes equations, effectively capturing unsteady aerodynamics and acoustics. Detailed methodologies are referenced in Naseer *et al.* (2023), Arif *et al.* (2023), and Lam *et al.* (2014). The dynamic behavior of an elastic panel under aeroacoustic loads was modeled using a simplified one-dimensional plate equation, integrated into our comprehensive monolithic scheme to handle nonlinear aeroacoustic–structural interactions (further details in Arif *et al.*, 2020; Fan *et al.*, 2018). Our calculations focused on a deep cavity with a length-to-depth ratio $L/D = 0.4$, subjected to a freestream velocity of 30 m/s, known for significant noise production. The computational setup, depicted in Fig. 2(a), utilized appropriate boundary conditions and a structured grid of 2.74×10^6 elements to ensure precise resolution of flow dynamics and acoustic propagation. Mesh convergence and additional computational specifics are discussed in Naseer *et al.* (2023). Figure 2(b) illustrates the setup of virtual probe locations critical for analyzing cavity acoustics, structural dynamics, and far-field noise. Our numerical results were validated against experimental data from Yokoyama *et al.* (2020), demonstrating strong agreement in acoustic phenomena and SPL measurements, with detailed findings shown in Fig. 3 and summarized in Naseer *et al.* (2023).

III. CAVITY–PANEL CONFIGURATIONS WITH SINGLE PANEL

A. Determination of potential panel locations

In order to appropriately mount the elastic panels for the proposed noise suppression approach, it requires certain knowledge of the flow characteristics over the rigid cavity from which the potential panel locations to achieve resonance conditions for modifying the cavity feedback mechanism can be deduced. Our previous study (Naseer *et al.*, 2023) on the rigid cavity noise outlines the physical processes that lead to the aeroacoustic feedback coupling between the cavity shear layer and the cavity acoustic mode, responsible for the ultimate intense tonal noise radiation. The results pinpoint that each cavity wall supports a certain physical process that maintains the aeroacoustic feedback coupling. Thus, to modify the identified coupling phenomena

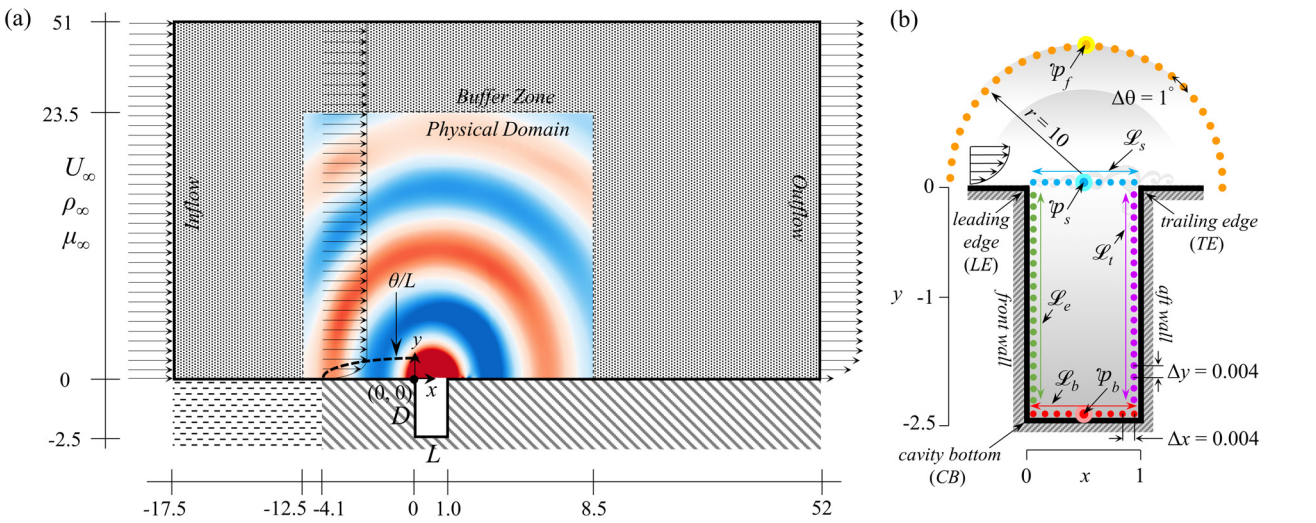

FIG. 2. (a) Schematic representation of the physical problem (not to scale). (b) Virtual probe locations around the cavity. Checkpoints indicated with distinctive lines, i.e., $\mathscr{L}_s$: (0,0) → (1,0), $\mathscr{L}_b$: (0,–2.5) → (1,–2.5), $\mathscr{L}_e$: (0,0) → (0,–2.5), and $\mathscr{L}_t$: (1,0) → (1,–2.5). The reference points of correlation analysis in subsequent discussions are p_f: (0.5, 20), p_s: (0.5, 0), and p_b: (0.5, −2.5).

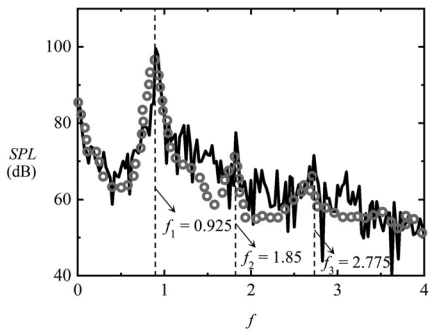

	Dominant frequency, f_1	$SPL(f_1)$
Present	0.925	99.6 dB
Yokoyama *et al.* (2020)	0.94 (-1.6%)	99 dB (+0.6 dB)
Heller & Bliss (1975)	0.972 (-4.8%)	---

FIG. 3. Comparison of acoustic spectra at $(x, y) = (6.75, 21.5)$ obtained from the study of Yokoyama *et al.* (2016, 2017, 2020) and the numerical calculation. solid line, Present; ◦, Experiments. In the table, the values in brackets show the relative changes of the present numerical results from respective experimental and theoretical values. *SPL* is defined relative to 20 μPa.

for the ultimate noise suppression, we attempted five cavity-panel configurations [Fig. 4(a)] so that each elastic panel could interact with an aeroacoustic coupling process and absorb the incident flow fluctuation energy to maintain its flow/acoustically induced vibration. The deterministic consideration of this modification strategy is the natural frequency of the elastic panel in the presence of fluid loading, which must be kept the same as the dominant frequency of the rigid cavity (*RC*) flow. In order to achieve the fluid-loaded panel natural vibration with fixed end boundary conditions, Eq. (1) is used. While keeping the panel length same as the cavity length, the thickness and the exerted tension can be altered to match the designed frequency. All panels are assumed to be made up of elastomeric material like silicon rubber following the suggestions of a previous study (Naseer *et al.*, 2022). Table I shows the three panel designs that are considered. Their target designed natural frequencies for the noise control actions are selected to be the third ($n = ③$) resonant modes of the panels, which are highlighted and shaded in the table. The rationale behind the choice of these three specific natural frequencies will be elaborated upon in the upcoming discussions,

$$(f_{EPdX})_n = \frac{n}{2L}\sqrt{\frac{T_{EP}}{\rho_{EP}h_{EP}}}\Big/\sqrt{1+\frac{L_{EP}}{\pi n \rho_{EP}h_{EP}}}. \quad (1)$$

B. Cavity noise reduction

Figure 4(b) shows the vibratory response of every single panel as it interacts with the cavity flow. The temporal patterns of sustained panel vibration reflect the successful execution of our conceived idea of flow fluctuation energy extraction through flow/acoustically triggered panel vibration. The extent of ultimate noise reduction or amplification varies across different cavity-panel configurations. The *SPL* spectra measured at the far field reveal that the flow-induced resonant panel vibrations mitigate most effectively the cavity tonal noise when the panel is mounted either at the aft or the bottom wall of the cavity as the respective peak *SPL* reduction of 3.8 and 3.6 dB from the *RC* case is observed. The azimuthal *SPL* distribution shows consistent reduction pattern. It can also be seen that the best performing cases are associated with a shift in the cavity flow dominant frequency from 0.925 to 1.25. For the detailed reasoning of the cavity-panel configuration noise reduction mechanisms, readers are referred to Naseer *et al.* (2023). However, to aid the understanding of the present study, the noise reduction mechanisms are succinctly explained here. The dominant frequency shift in EP_{aft} case is attributed to the energy absorption of the dominant low-frequency mode by the vibrating panel, resulting from the interaction of the shear layer vortices with the aft panel. The dominant frequency shift in EP_{bottom} case is attributed to the energy absorption of the dominant low-frequency modes by the vibrating panel, resulting from the incidence of acoustic waves on the bottom panel. After absorbing the flow excitation energy of the low-frequency mode, the flow-panel interaction shifts the frequency to a higher mode of lesser energy, which emerges as the new flow dominant mode. Furthermore, the interaction also invokes the phase shift in the coupling between the shear layer and cavity acoustic mode. As a result, when the reflected acoustic waves from the cavity bottom meet the shear layer at the cavity opening, it excites the shear layer according to the shifted mode, but it does not support the favorable mutual phase difference ($\Delta\phi \sim 0$) near the cavity leading edge as occurred in *RC* case. These two actions result in a delayed shear layer growth. Hence, the effectively shortened shear layer length also assists the shift in the previously sustained Rossiter frequency of $f = 0.925$ to the higher mode of $f = 1.25$ for EP_{aft} and EP_{bottom} case. In summary, the cavity-panel configuration with single panel has shown its effectiveness in reducing the aeroacoustically generated deep cavity noise, given that the location of the elastic panel is appropriately designed and located.

IV. CAVITY–PANEL CONFIGURATION WITH MULTIPLE PANELS

Cavity-panel configurations with a single elastic panel have shown promising noise reduction potential. To leverage further noise suppression, the present study attempts an extended approach based on configurations with multiple panels (Fig. 5). We first formulate the configurations with double panels (*DEP*) by combining the best-performing single-panel cases in Sec. III with differently designed frequency arrangements. A *DEP* configuration is designed in such a way that an elastic panel is mounted on the aft wall, whereas another panel is mounted at the cavity bottom. Each *DEP* configuration is uniquely assigned a combination of panel natural frequencies based on aeroacoustical physics identified in *RC* case and previously tested cases with single panels. To design the panels for *DEP*, there are two frequencies of interest. The first is the original frequency of *RC* tone ($f = 0.925$) and the second is the shifted frequency ($f = 1.25$), which emerges

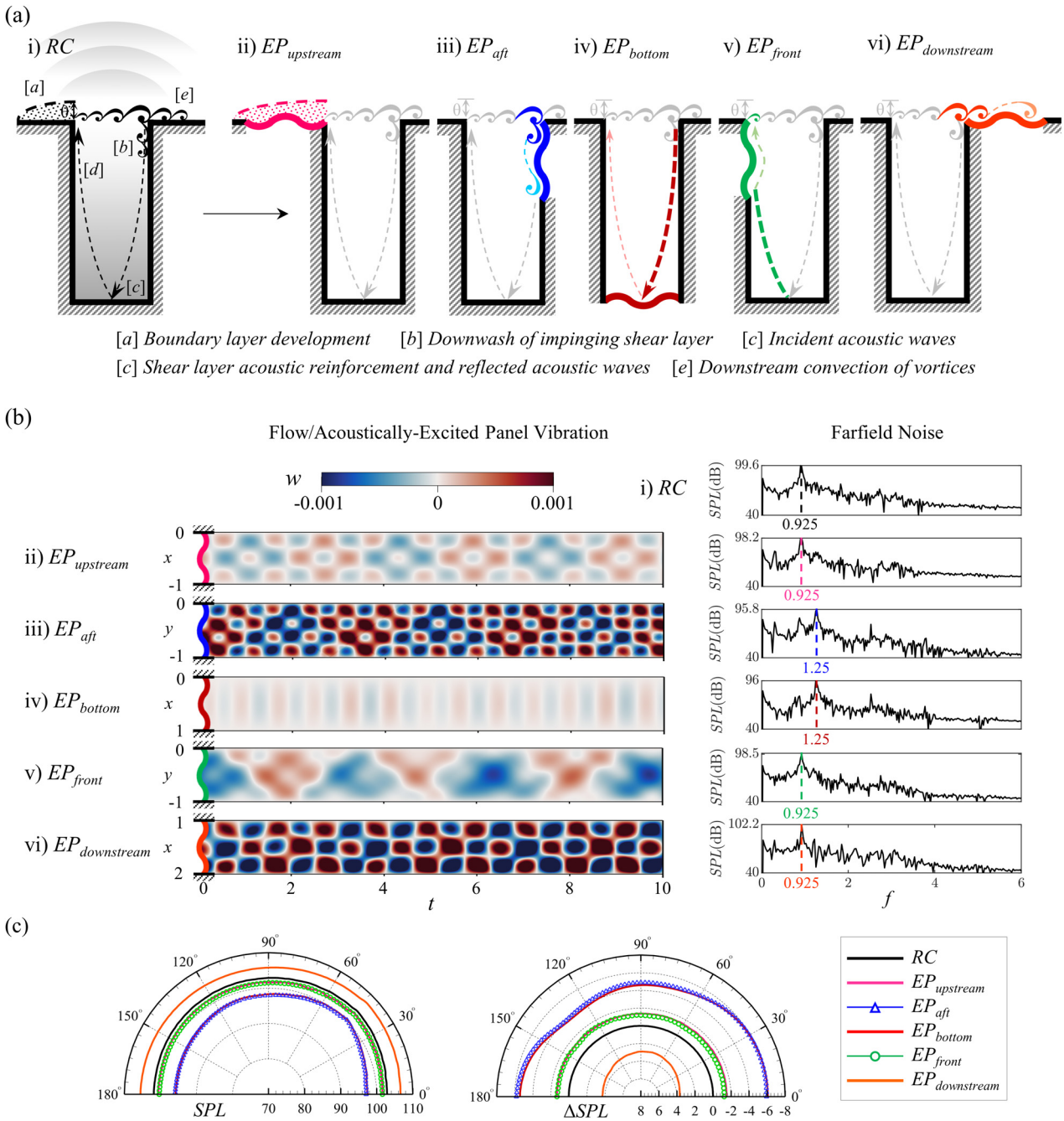

FIG. 4. Cavity noise suppression with strategic modification of shear layer–acoustic mode coupling using single elastic panel. (a) Identified key physical processes responsible for feedback mechanism (Naseer *et al.* 2023) and the panels (ii)–(vi) set for the individual processes [a]–[e] for modifying the feedback. (b) Flow/acoustically excited panel vibratory responses exhibiting the significant flow energy extraction and its effect on the far-field cavity tone at $(x, y) = (6.75, 21.5)$ and its frequency shift. (c) Azimuthal distributions of *SPL* of different cavity-panel configurations and their noise reduction ΔSPL.

when a single elastic panel operates at either the aft or the cavity bottom wall (as discussed in Sec. III). *DEP*1 configuration simply combines the *SEP*1 and *SEP*2 panels whose natural frequencies are tuned to meet the dominant frequency of *RC* case. The combined actions of the panels on the shear layer and the cavity acoustic mode are envisaged to doubly effect the resultant noise reduction. As seen in Naseer *et al.* (2023), the panel at the aft or the bottom cavity wall tends to shift the dominant cavity aeroacoustic fluctuation mode from $f = 0.925$ to

TABLE I. Three panel designs and the distribution of the first nine resonant modes of each design.

		*n*th resonant panel frequency								
	$n =$	①	②	③	④	⑤	⑥	⑦	⑧	⑨
Panel design	f_{EPd1}	0.306	0.615	0.925	1.234	1.54	1.852	2.16	2.47	2.78
	f_{EPd2}	0.414	0.832	1.25	1.668	2.086	2.5	2.92	3.3	3.75
	f_{EPd3}	0.455	0.915	1.375	1.835	2.295	2.75	3.21	3.67	4.13

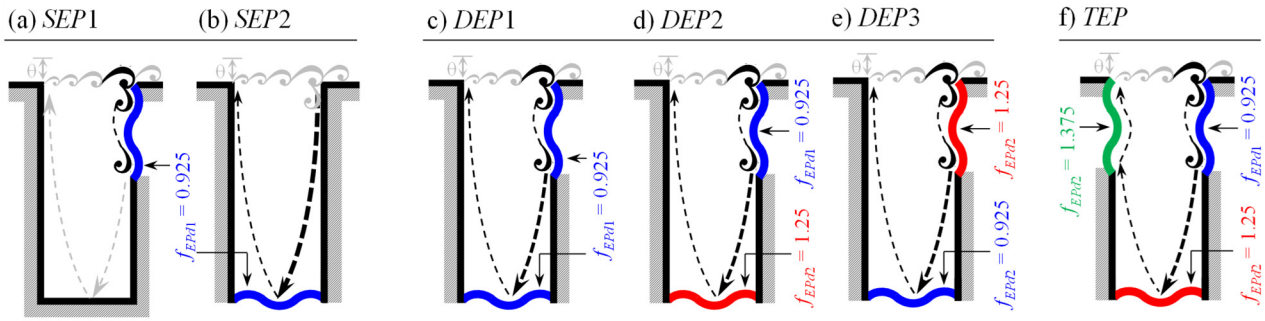

FIG. 5. Cavity configurations with multiple panels. Note that the EP_{aft} and EP_{bottom} cases in Fig. 4 are renamed as *SEP*1 and *SEP*2 for the sake of consistency of forthcoming discussions. (a) *SEP*1, (b) *SEP*2, (c) *DEP*1, (d) *DEP*2, (e) *DEP*3, and (f) *TEP*.

$f = 1.25$. Therefore, another *DEP* configuration has been designed in which one panel is to cater the original *RC* dominant frequency, $f = 0.925$ and another is for the shifted frequency ($f = 1.25$). In this way, when one panel triggers the frequency shift after pacifying the energy-enriched content at $f = 0.925$ of the flow, the other panel should be accordantly designed to interact with the shifted mode. Following this approach, *DEP*2 and *DEP*3 configurations are considered. In *DEP*2, the aft panel is designed to target the original *RC* frequency, whereas the bottom panel is tuned to comply with the envisaged shifted frequency. In *DEP*3, the targeted actions of the two panels with respect to the selected frequencies are swapped. To seek further possibility for more cavity noise reduction, a triple elastic panel configuration (*TEP*) is also attempted by mounting one more panel at the cavity front wall in *DEP*2 configuration. Since the dominant frequency observed in *DEP*2 is shifted to $f = 1.375$, this frequency is designated for the natural frequency of the third panel. As such, seven cases are discussed in this study along with the *RC* baseline case.

V. MODIFICATIONS OF CAVITY AEROACOUSTICS

The temporal evolution of flow pressure fluctuations p' within the cavity of all cases is depicted in Fig. 6. The figures reveal periodic flow fluctuations both along the shear layer region and inside the cavity. For easy comparison, the series of snapshots in each case commences at the moment of minimum pressure within the cavity. The subsequent snapshots are consistently taken at time intervals of $T/4$ within a single flow fluctuation period T of the dominant frequency captured at cavity bottom center $(x, y) = (0.5, -2.5)$. Note that the value of T varies and is accordingly shown for the tested cases. Evidently, the p' fluctuates in a clear alternating pattern in time with a spatial extent almost filling up the entire cavity. It is worth highlighting that a notable rarefaction ($p' < 0$) occurs concurrently at the moment $\sim T/4$ when the downwash secondary vortex forms (Fig. 7) as the flow separates at the cavity trailing edge. Subsequently, a significant compression wave ($p' > 0$) is generated (Fig. 6) after these two flow processes conclude ($\sim 3T/4$). These findings are consistent with the results of a previous numerical investigation of flow past a deep cavity of almost similar size (Ho and Kim, 2021). The fluctuation patterns of p' within the cavity depicted in Fig. 6 are identified as the cavity acoustic mode (Naseer *et al.*, 2023). When this cavity acoustic mode interacts with the shear layer at the cavity opening, it promotes strong acoustic radiation (Fig. 8) specifically for the *RC* case. A close examination of Fig. 6 reveals a strong pressure fluctuation due to cavity mode oscillation in the *RC* case. However, in all the cases with elastic panels, the intensity of these fluctuations is markedly diminished.

In Fig. 7, we can observe a fluctuating shear layer originating from the cavity leading edge [*LE* in Fig. 2(b)]. This shear layer gives rise to a sequence of substantial vortical flow structures as a result of Kelvin–Helmholtz instabilities that convect downstream. When these streamwise growing vortical structures reach the cavity trailing edge [*TE* in Fig. 2(b)], their strong vortex–structure interaction results in the emergence of separating flow over the flat wall downstream of the cavity. Meanwhile, the intensified strain rate induced near *TE* generates a series of secondary vortical structures that extends and descends into the cavity. As these secondary vortical structures detach from the *TE*, the strain rate diminishes and the high vorticity region contracts as the flow progresses along the cavity aft wall. Among all the cases under consideration, with or without panels, the oscillation patterns of the shear layers across the cavity opening remains more or less the same. However, a noteworthy observation in comparison to the *RC* case is the delayed shear layer growth in all cases with elastic panels. This

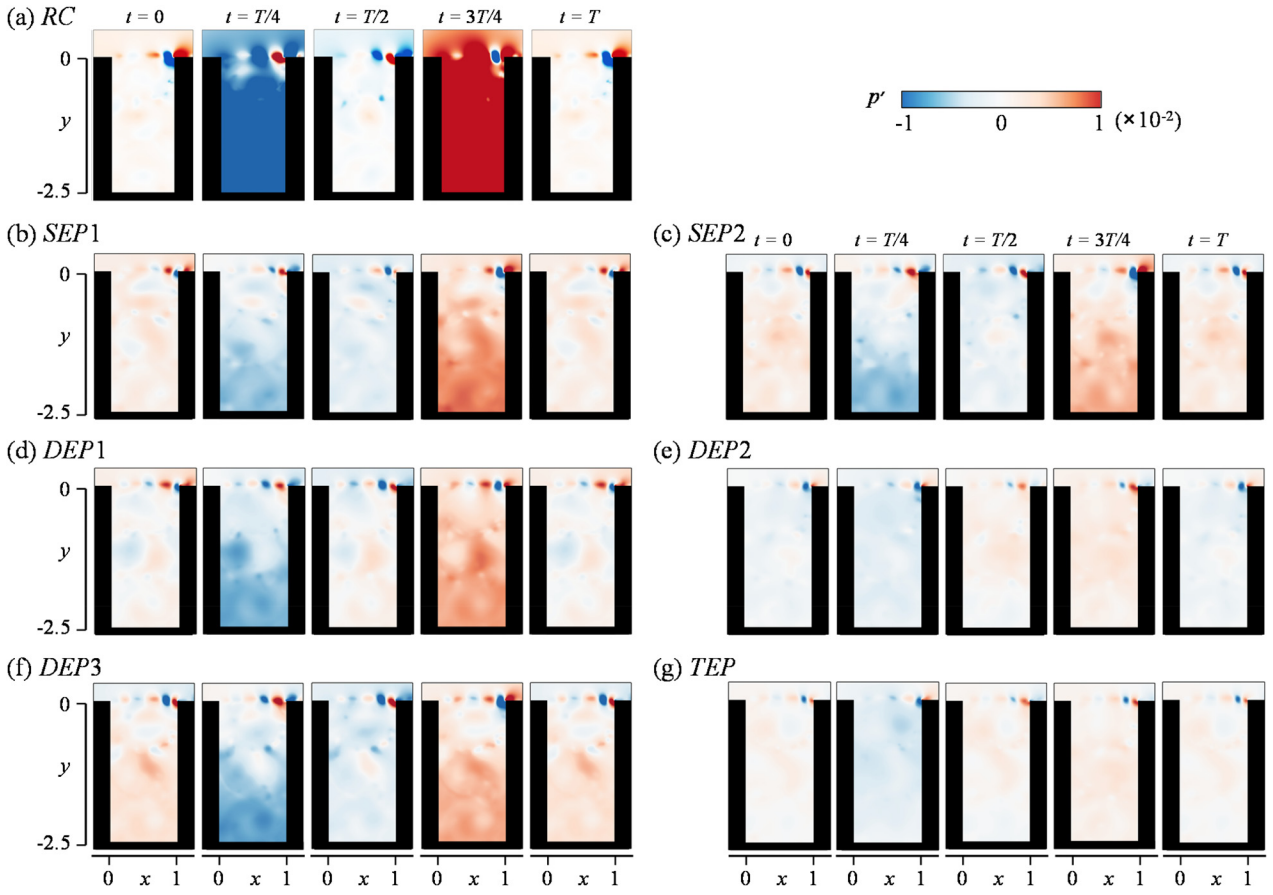

FIG. 6. Snapshots of instantaneous pressure fluctuation p' for a cycle of cavity mode oscillation, commencing from the moment of shear layer impingement at the downstream edge. (a) *RC*, (b) *SEP*1, (c) *SEP*2, (d) *DEP*1, (e) *DEP*2, (f) *DEP*3, and (g) *TEP*.

delayed growth is not merely a minor variation, but rather a significant one, suggesting a potential alteration in the feedback phenomena in these cases.

In Fig. 8, we can observe the snapshots of instantaneous p' of noise radiation for all configurations, taken at the moment when the acoustic rarefaction impacts the cavity bottom. As depicted, the cavity noise is tonal in nature and resembles the *RC* radiation. However, the magnitude of noise radiation varies substantially across all cases. *DEP*2 and *TEP* cases exhibit the highest acoustic reduction whereas a slight reduction in noise is observed in all the remaining cases.

Figure 9 shows a comparison of noise spectra at p_f in far-field and at p_b near cavity bottom, with the power spectral density (*PSD*) of p' at p_s within shear layer. We can see that the *DEP*1 and *DEP*3 cases give the lowest noise reduction from the *RC* case, whereas the *SEP*1 and *SEP*2 cases give moderate reduction and *DEP*2 and *TEP* give the highest reduction. A closer look at the spectra reveals a distinct trend concerning the frequency peaks. A single peak at $f = 1.25$ dominates the spectra in *SEP*1, *SEP*2, *DEP*1, and *DEP*3 cases regardless of the measurement locations. On the other hand multiple peaks, namely at $f = 0.925$, 1.25, and 1.375, dominate the spectra across various locations in the *DEP*2 and *TEP* cases. These findings indicate that despite the shift in dominant frequency from $f = 0.925$ to $f = 1.25$ in some cases (*SEP*1, *SEP*2, *DEP*1, and *DEP*3), the aeroacoustic coupling between the shear layer fluctuation and the cavity acoustic mode remains intact. This is due to the fact that both the shear layer and acoustic mode are locked-on together and operating at similar frequencies, as evidenced by the corresponding spectra at p_s and p_b. Similar frequency lock-in phenomenon was observed in many studies of rigid cavity flow (East, 1966; Yang *et al.* 2009; Yokoyama *et al.*, 2017; and Ho and Kim, 2021).

On the contrary, in the *DEP*2 and *TEP* cases, the aeroacoustic coupling appears to disintegrate entirely. This is reflected from the fact that the shear layer and cavity mode operating at dissimilar frequencies, thereby failing to meet the conditions necessary for shear layer-cavity mode coupling. This results in a significant reduction in cavity tonal noise by 15 dB from the *RC* case. The far-field noise p' spectra of *DEP*2 and *TEP* reveal a mismatch frequency interaction between the shear layer and cavity mode, producing three distinct frequency peaks ($f = 0.925$, 1.375, and 0.45) of nearly equal magnitude. These peaks originate from the cavity mode, shear layer, and their interaction ($f = 0.45 = 1.375–0.925$), respectively. This suggests that the far-field noise reduction can be best achieved by initially shifting the shear layer

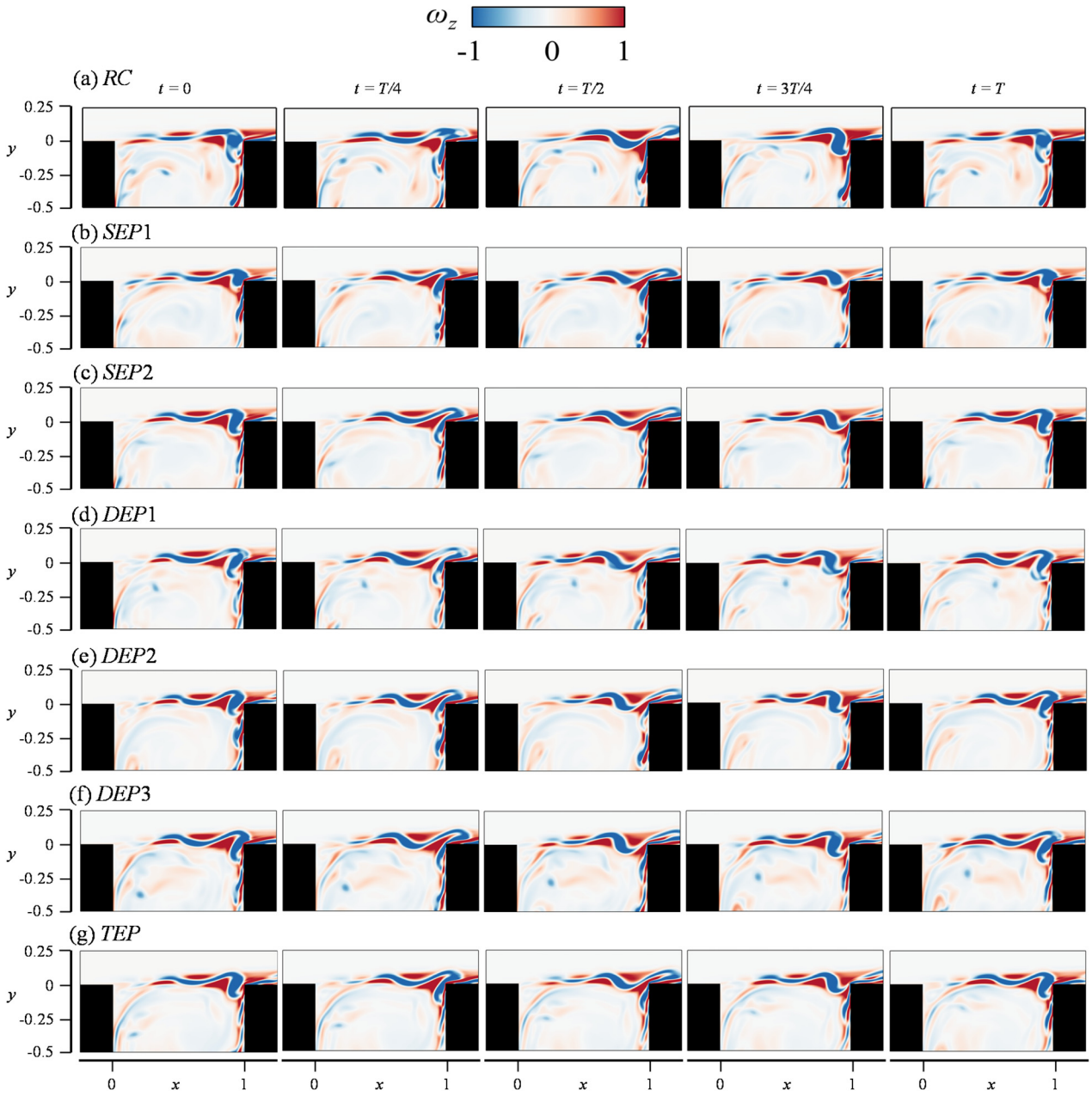

FIG. 7. Instantaneous vorticity during the shear layer growth, followed by the downwash after impingement near the cavity opening region, spanning a full shear layer oscillation cycle. Snapshots are synchronized with those in Fig. 6. (a) *RC*, (b) *SEP*1, (c) *SEP*2, (d) *DEP*1, (e) *DEP*2, (f) *DEP*3, and (g) *TEP*.

frequency to a higher mode via the aft panel, followed by pacifying the shifted cavity mode through the bottom panel using suitably designed panel frequencies. In this context, the *DEP*2 configuration appears to be particularly effective.

Figure 10 shows the azimuthal *SPL* distributions of all the cases extracted at the respective peak frequencies. All the cavity noise directivity patterns closely resemble the *RC* case. Notably, the *SEP*1 and *SEP*2 cases introduce a slight directivity shift which results in a new peak radiation angle at approximately 45° from the downstream horizontal wall. The azimuthal variation of *SPL* in *DEP*1, *DEP*3, and *TEP* exhibit relatively consistent behaviors. However, the extent of noise reduction in *DEP*2 displays high variation across different azimuthal angles. The efficacy of noise reduction by the elastic panels can be quantified using the change in sound power level $\Delta PWL = 10\log_{10}(W_{EP}/W_{RC})$, in dB, where $W = \int_0^{\pi} p'_{rms} d\theta$. Notably, the *SEP*1, *SEP*2, and *DEP*1 cases achieve a mild sound power reduction of

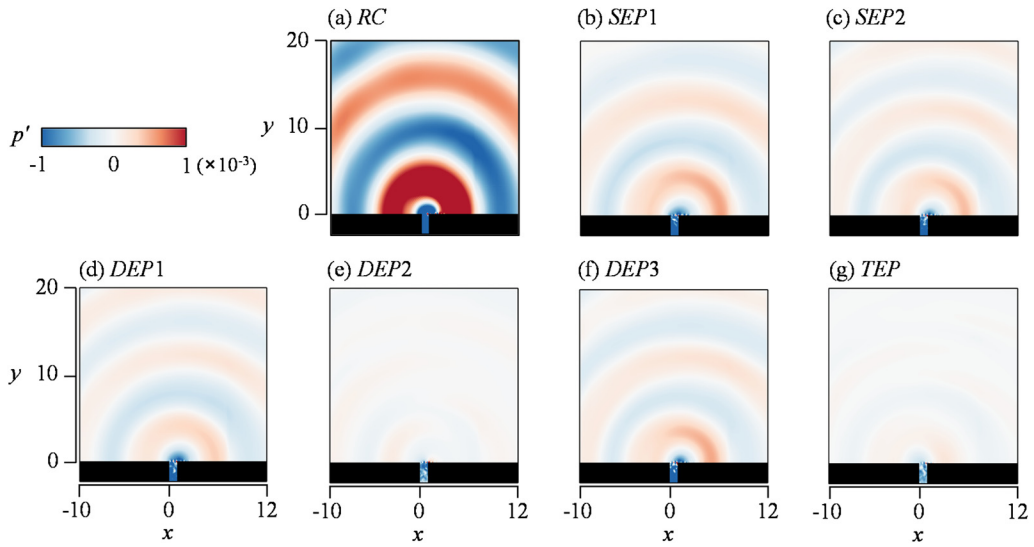

FIG. 8. Instantaneous noise radiation captured at the instant of cavity mode rarefaction hits the cavity bottom (i.e., at $\sim T/4$ of Fig. 6). (a) *RC*, (b) *SEP*1, (c) *SEP*2, (d) *DEP*1, (e) *DEP*2, (f) *DEP*3, and (g) *TEP*.

nearly 5 dB, but the *DEP*2 and *TEP* cases demonstrate a remarkable sound power level reduction of 14.3 and 13.6 dB, respectively [Figs. 9(e) and 9(g)]. In summary, these observations provide robust evidence that the cavity-panel configurations designed with panels of dissimilar resonant frequencies exhibit much prominent cavity noise reduction than the configurations designed with the same/similar frequencies. The forthcoming section will delve into the analysis and discussion of the physical mechanisms underlying these phenomena.

It is intriguing to examine the impact of elastic panels on the time-averaged drag experienced by the cavity (Table II), calculated using the method adopted by Gharib and Roshko (1987) as $\bar{C}_D = 2\bar{F}_d/\rho u^2 l_{(x,y)}$, where $\bar{F}_d = \bar{F}_{form} + \bar{F}_{fric}$; $\bar{F}_{form} = -\int_{-2.5}^{0} p(0,y)\,dy + \int_{-2.5}^{0} p(1,y)\,dy$; and $\bar{F}_{fric} = \int_{0}^{1} \tau(x,-2.5)\,dx$. Notably, the skin friction drag coefficient $\bar{C}_{D,fric}$ is two orders of magnitude weaker than the form drag coefficient $\bar{C}_{D,form}$ in all cases so the latter is the primary contributor to the total cavity drag $\bar{C}_D$. For all the configurations in the study, a consistent reduction in total drag, up to 20%, from the *RC* case is observed. In particular, the quietest *DEP*2 and *TEP* configurations give a total drag reduction of ∼16% and ∼11%, respectively. The use of elastic panels for noise reduction is remarkably accomplished without compromising the cavity aerodynamics. In fact, it offers the advantage of reduced cavity drag. It is worth noting that similar aeroacoustic benefits have been observed in the context of utilizing flow-induced elastic panels for tonal noise reduction in airfoils (Arif *et al.*, 2022).

VI. NOISE SUPPRESSION MECHANISM WITH MULTIPLE PANELS

Figure 11 shows the variations of pressure fluctuation p' along the lines $\mathscr{L}_s$ and $\mathscr{L}_b$ [in Fig. 2(b)] to illustrate the spatial-temporal variations of the shear layer growth across the cavity opening and cavity acoustic mode behavior at the cavity bottom, respectively. The inclined ridges in first column of Fig. 11 highlight the downstream convecting shear layer vortices and their convective velocities are estimated by the slope of the dashed lines. By utilizing the estimated values for vortices convection velocity ($\kappa \sim 0.5$, 0.67, and 0.72) and the suggested negligible phase delay ($\alpha \sim 0$) between the impinging vortex and acoustic emission (Forestier *et al.*, 2003; Larchevêque *et al.*, 2003; and El Hassan *et al.*, 2008), the modified formula for Rossiter modes (Naseer *et al.*, 2023) is employed to determine that the second ($m = 2$) dominant mode dominates the flow regimes across the cases. The resulting frequencies are $f = 0.95$, 1.26, and 1.375. These values agree well with the dominant shear layer frequencies observed in the pressure spectra in all the cases (Fig. 9). This agreement suggests that the cavity-panel configurations do not undergo significant alterations of the fundamental shear layer dynamics and continue to adhere to the inherent cavity flow behavior. This behavior can be effectively elucidated and supplemented by the established methodologies.

When the shear layer impinges at the cavity trailing edge, it emits acoustic waves that travel toward the cavity bottom and reflect upward along the cavity to form a standing wave for its acoustic mode whose existence is confirmed in the second column of Fig. 11. A comparison of strength of cavity standing waves reveals that the *RC* configuration gives robust internal cavity fluctuations. In contrast, the *DEP*2 configuration appears to significantly reduce the acoustic mode footprints as a result of an effective acoustic energy loss to the resonant panel at cavity bottom. Other panel configurations appear to keep similar cavity acoustic fluctuations to certain extent, albeit at significantly lower magnitudes than in *RC* case.

Upon examining the relationship between the strength of the shear layer (near the cavity trailing edge) and the cavity mode in each case, an inverse correlation is observed: the weaker the cavity mode, the stronger the shear layer. This phenomenon can be explained by the aeroacoustic feedback mechanism proposed by Bruggeman *et al.* (1989). It is conceptualized on the energy transfer between the vortical (hydrodynamic) and potential (acoustic) fields in their study of the noise response of a flow-induced oscillation at low Mach number

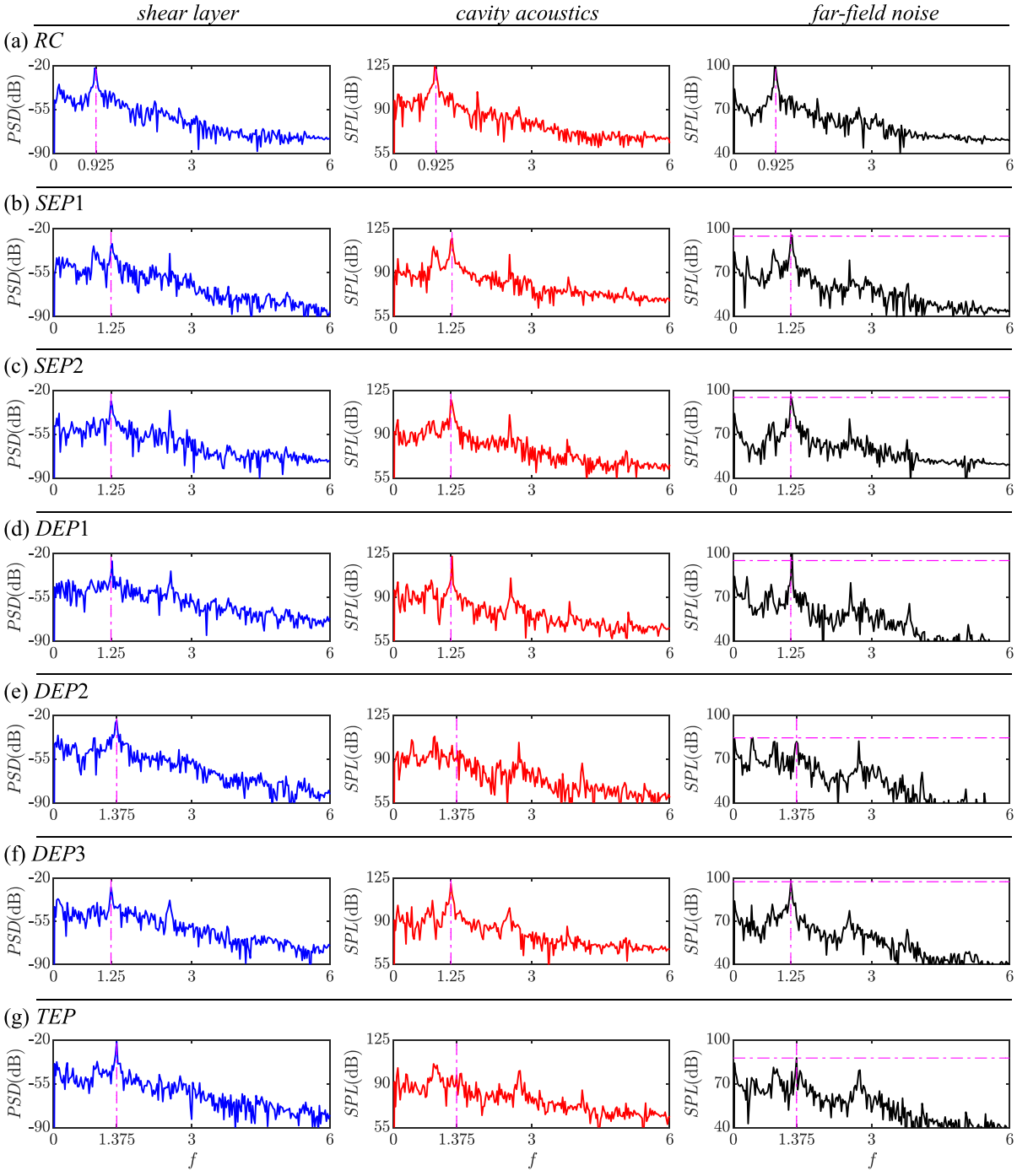

FIG. 9. Comparison of p' spectra measured at locations p_s (first column), p_b (second column), and p_f (third column). The vertical dashed lines indicate the dominant frequencies trending across different cases and different sample locations. (a) *RC*, (b) *SEP*1, (c) *SEP*2, (d) *DEP*1, (e) *DEP*2, (f) *DEP*3, and (g) *TEP*.

(0.07) in closed side-branches of the gas transport system. In their theoretical framework, based on the concept of the vortex sound theory (Powell, 1964; Howe, 2003), Bruggeman presented the feedback mechanism constituted by the following processes: acoustic forcing from the resonance on the shear layer at the upstream corner; formation of coherent vortices by the instabilities in the separated shear layer; transfer of energy from the local flow to the acoustic field by the interaction of convective vorticity and the acoustic resonance; and the net energy

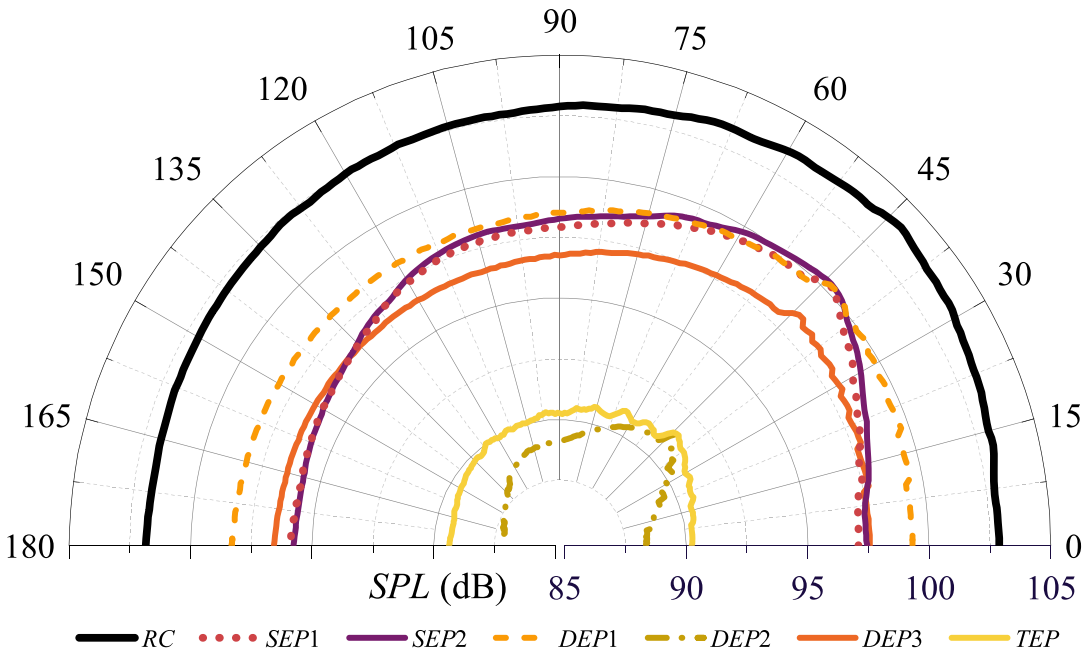

Cases	*SEP*1	*SEP*2	*DEP*1	*DEP*2	*DEP*3	*TEP*
ΔPWL (dB)	− 4.6	− 4.8	− 5.1	− 14.3	− 3.2	-13.6

FIG. 10. Azimuthal distribution of peak *SPL* at $r = 10$. The table illustrates the changes in sound power level from *RC* case.

TABLE II. Comparison of skin friction drag $\bar{C}_{D,fric}$, form drag $\bar{C}_{D,form}$, and total drag $\bar{C}_D$ for all cavity-panel configurations. Values in brackets indicate the percentage deviations from the *RC* case.

	$\bar{C}_{D,fric}$	$\bar{C}_{D,form}$	$\bar{C}_D$
RC	5.68×10^{-5}	1.70×10^{-3}	1.76×10^{-3}
*SEP*1	6.48×10^{-5} (+14.1%)	1.36×10^{-3} (−20.2%)	1.42×10^{-3} (−19.1%)
*SEP*2	5.48×10^{-5} (−3.6%)	1.59×10^{-3} (−6.4%)	1.64×10^{-3} (−6.4%)
*DEP*1	5.56×10^{-5} (−2.1%)	1.64×10^{-3} (−3.5%)	1.69×10^{-3} (−3.9%)
*DEP*2	5.15×10^{-5} (−9.26%)	1.43×10^{-3} (−15.7%)	1.48×10^{-3} (−15.6%)
*DEP*3	5.6×10^{-5} (−1.4%)	1.67×10^{-3} (−2.2%)	1.73×10^{-3} (−1.9%)
TEP	5.66×10^{-5} (−0.3%)	1.51×10^{-3} (−11.4%)	1.57×10^{-3} (−10.9%)

transfer to the acoustic field determines the amplitude and the phase of the feedback at the upstream corner. Similar observations have also been reported in other studies (Yang *et al.*, 2009; Yamouni *et al.*, 2013; and Ho and Kim, 2021).

As illustrated in Fig. 11(a), the said feedback mechanism is evident in the *RC* configuration, where the maximum shear layer energy appears to be converted to the acoustic mode at the resonance frequency $f = 0.925$. The superimposed vertical dashed lines indicate the acoustic mode meeting the in-phase shear layer convective ridges on the upstream edge ($x \sim 0$). However, the cavity-panel configurations deviate from this behavior due to potential phase modifications of the cavity mode induced by the elastic panel. In fact, across the cavity opening, the out-of-phase destructive interference between the growing shear layer and passing acoustic waves appears to delay the shear layer growth in the *DEP*2 and *TEP* configurations. This is evidenced by the observation of a region of stagnant or stationary flow ($p' \sim 0$) around $x \sim 0.3$ in these cases [Figs. 11(e) and 11(g)], where the horizontal dashed lines indicate the interruption of shear layer growth due to destructive interference upon the out-of-phase shear layer-cavity mode interaction.

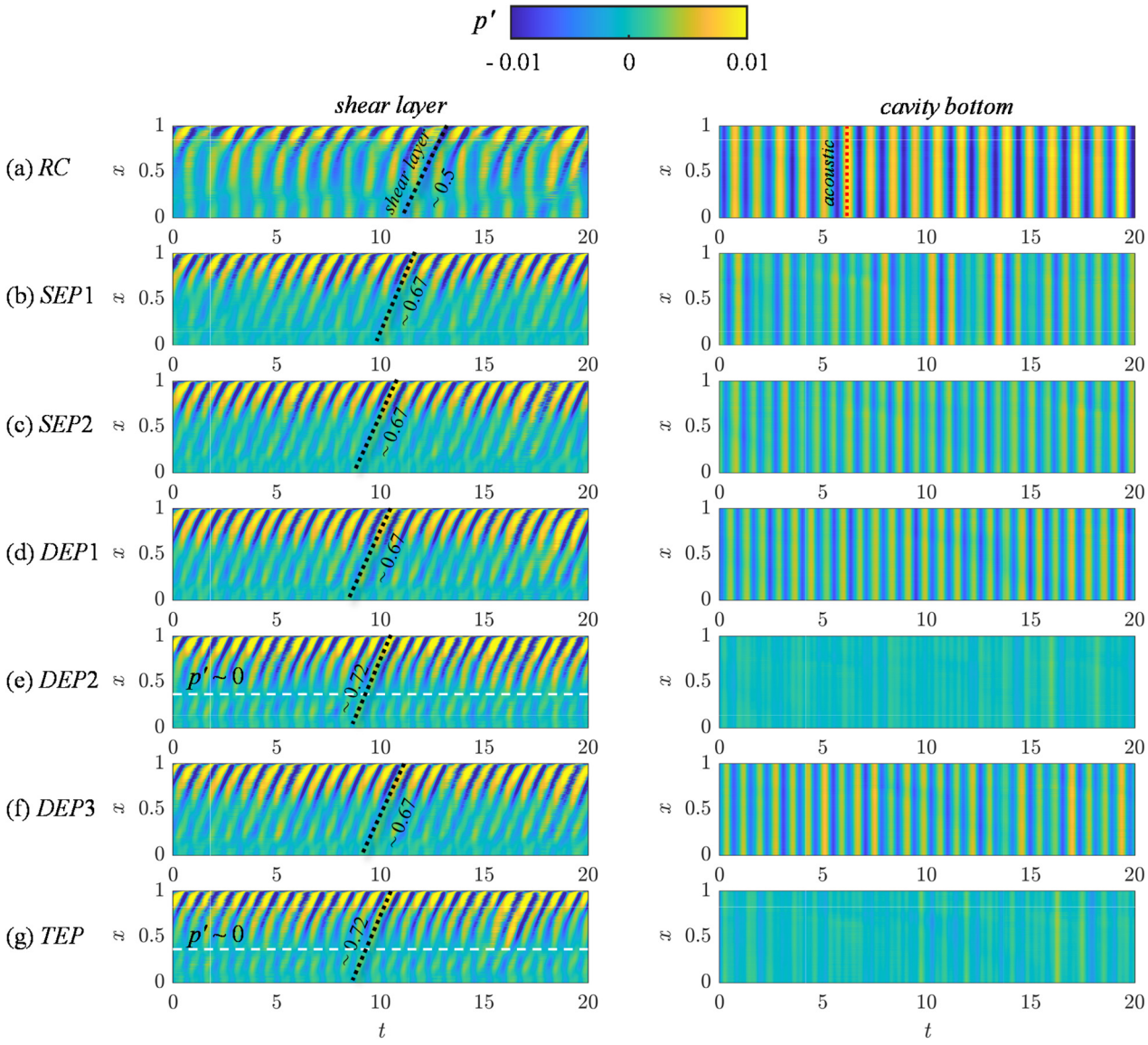

FIG. 11. Temporal variations of p' across the cavity shear layer ($\mathscr{L}_s$) and along the cavity bottom ($\mathscr{L}_b$). The slope of inclined ridges marked with dashed lines measures the vortex convection velocity, and vertical dashed lines mark the projection of the corresponding cavity mode. (a) *RC*, (b) *SEP*1, (c) *SEP*2, (d) *DEP*1, (e) *DEP*2, (f) *DEP*3, and (g) *TEP*.

Our observations indicate that the feedback mechanism driving the deep cavity flow and generating the extreme acoustic response in the *RC* case is a result of the mutual interaction between the convective shear layer and the cavity acoustic mode. This interaction occurs at the same frequency and their favorable phase relationship (a lock-on effect), which facilitates maximum energy conversion from the shear layer to the cavity acoustics. However, in the *SEP*1, *SEP*2, *DEP*1, and *DEP*3 cases, although the shear layer and cavity mode are fluctuating at a similar frequency, their acoustic radiation is slightly reduced whereas in *DEP*2 and *TEP* cases the significant acoustic reduction is accompanied by the emergence of different shear layer and cavity mode fluctuation frequency as observed in Fig. 9. To understand the dynamics leading to this acoustics reduction, it is beneficial to examine the spatial distribution of p' spectra within the shear layer (i.e., along the $\mathscr{L}_s$) and on the cavity bottom (i.e., along the $\mathscr{L}_b$). Additionally, it is important to assess the coherence γ^2 between $p'(\mathscr{L}_s)$ and $p'(p_b)$ calculated as $\gamma^2(f) = |P_{sb}(f)|^2/P_s(f)P_b(f)$, where $P_s(f)$ and $P_b(f)$ are the power spectral densities of p' signals for the shear layer and the acoustic mode, respectively, and $P_{sb}(f)$ is the cross power spectral density between the signals. It is also prudent to evaluate the phase difference $\Delta\phi$ between $p'(\mathscr{L}_s)$ and $p'(\mathscr{L}_b)$ along same streamwise location (i.e., same x) (Fig. 12).

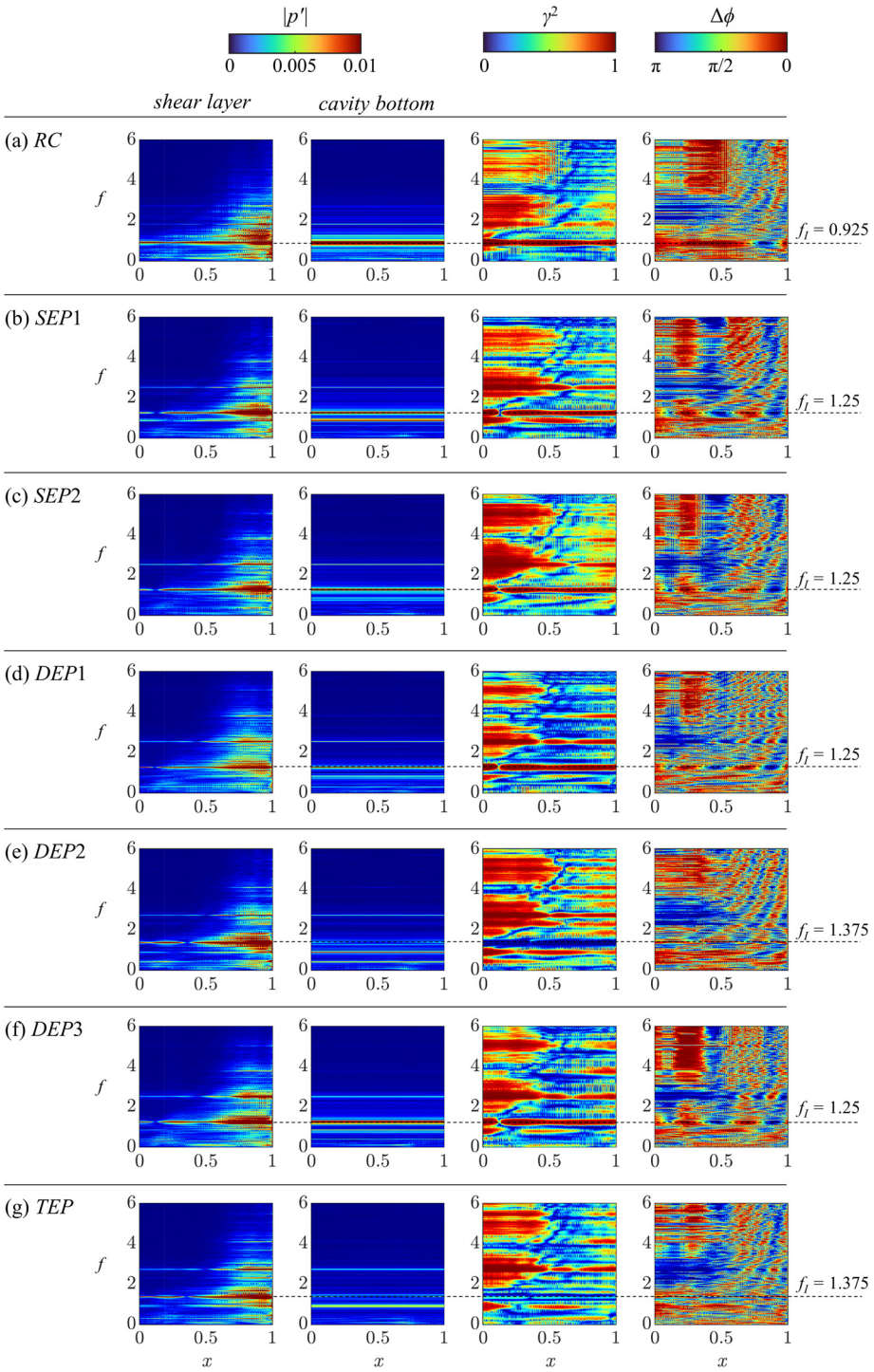

FIG. 12. First column: variation of FFT transformed $p'(\mathscr{L}_s)$ magnitude across cavity opening. Second column: variation of FFT transformed $p'(\mathscr{L}_b)$ magnitude across the cavity bottom ($\mathscr{L}_b$). Third column: coherence, γ^2 between shear layer pressure $p'(\mathscr{L}_s)$ across cavity opening and acoustic pressure at cavity bottom center $p'(p_b)$. Fourth column: phase difference, $\Delta\phi$ between $p'(\mathscr{L}_s)$ and $p'(\mathscr{L}_b)$. (a) *RC*, (b) *SEP*1, (c) *SEP*2, (d) *DEP*1, (e) *DEP*2, (f) *DEP*3, and (g) *TEP*.

In the *RC* case, the shear layer impingement excites a range of frequencies near the cavity trailing edge and produces a relatively wide spectrum. However, only one frequency, $f = 0.925$, is amplified and locked-on between the growing shear layer and cavity acoustic mode for their strong mutual synchronization, $\gamma^2(0.925) \sim 1$, and in-phase excitation, $\Delta\phi(0.925) \sim 0$. This perfect condition for aeroacoustic resonance allows the acoustic field to draw maximum energy from the growing shear layer, as evidenced by the higher magnitude of the acoustic spectrum at the cavity bottom.

Having understood the conditions of the feedback coupling mechanism in the *RC* case, we can now establish a criterion based on four quantifiable conditions derived from the *RC* case and compare them in the cases with panels.

C1. Frequency lock-on ($f_{\text{shear layer}} = f_{\text{acoustic mode}} = f_1$);
C2. Strong synchronization ($\gamma^2(f_1) \sim 1$);
C3. Favorable phase difference ($\Delta\phi(f_1) \sim 0$);
C4. Energy conversion from shear layer to acoustic field ($|p'(\mathscr{L}_b, f_1)| > |p'(\mathscr{L}_s, f_1)|$).

Interestingly, the *SEP*1, *SEP*2, *DEP*1, and *DEP*3 cases meet two of the four conditions as their respective shear layer and cavity mode share the same frequency ($f = 1.25$) and strong synchronization [$\gamma^2(1.25) \sim 1$]. However, they fail to maintain a favorable phase difference at the dominant frequency, preventing efficient energy transfer to the acoustic mode upon shear layer impingement. As a result, the shear layer remains concentrated near the downstream edge. In the *DEP*2 and *TEP* cases, none of the four conditions are met, indicating a complete decoupling of the feedback mechanism and resulting in the highest noise reduction. Other cases with elastic panel partially follow the feedback process so slight noise reduction is resulted.

The p' magnitudes at the dominant frequencies of the spectra in Fig. 12 are consolidated to provide further insight into the variations of the coupling patterns between the shear layer growth and the cavity acoustics (Fig. 13). In the *RC* case, the p' magnitude gradually increases from cavity leading edge up to $x = 0.8$ and beyond which it suddenly rises by almost 160% at cavity trailing edge [Fig. 13(a)]. However, the presence of elastic panels in all configurations seems to significantly alter the evolution of p' along the cavity shear layer. Most notably, the pressure fluctuations in the shear layer appear to decay downstream, nearly diminishing (i.e., $p' \sim 0$) at certain streamwise locations, and then increase rapidly toward the trailing edge, surpassing the *RC* case at $x > 0.6$. Interestingly, the p' values of all configurations, except for *DEP* and *TEP*, completely decay to zero at $x \sim 0.13$. The p' values of *DEP*2 and *TEP* become zero at a further downstream position, around $x \sim 0.36$. The distributions of p' magnitude along the cavity bottom in Fig. 13(b) reveal that the presence of elastic panels tends to suppress the development of cavity acoustics in all configurations, with the *RC*

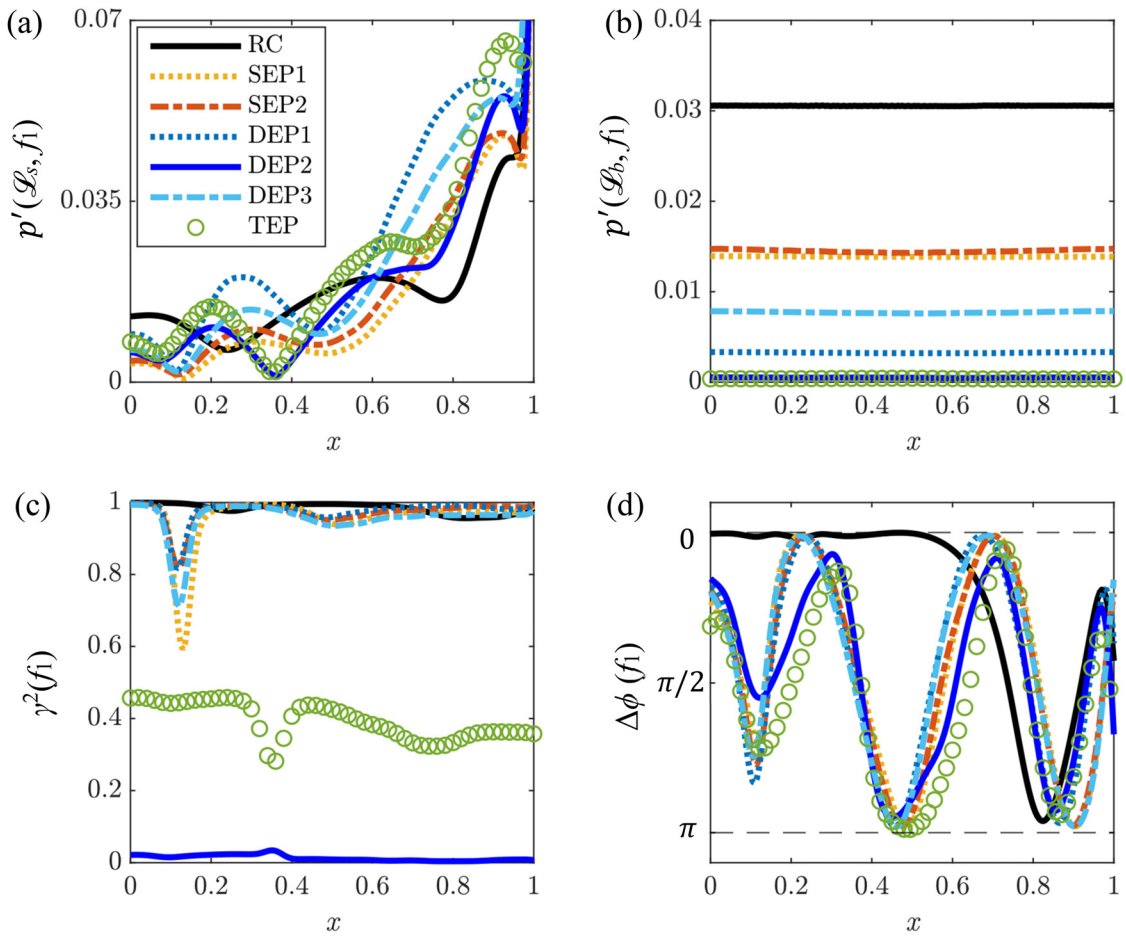

FIG. 13. (a) Variation of FFT transformed peak $p'(\mathscr{L}_s, f_1)$ magnitude across cavity opening. (b) Variation of FFT transformed peak $p'(\mathscr{L}_s, f_1)$ magnitude across the cavity bottom. (c) Coherence between shear layer pressure $p'(\mathscr{L}_s)$ across cavity opening and acoustic pressure $p'(p_b)$ at cavity bottom center. (d) Phase difference between $p'(\mathscr{L}_s, f_1)$ and $p'(\mathscr{L}_b, f_1)$.

case exhibiting the strongest cavity acoustics. The elastic panels are capable of reducing the acoustic p' at the cavity bottom by at least half. In particular, those in *DEP*2 and *TEP* can nullify the acoustic p', possibly due to the highly effective energy absorption by the resonant vibration of the panels at the cavity bottom.

To gain a better understanding of the aforementioned observations, it is more informative to study the coherence (γ^2) and the phase difference ($\Delta\phi$) of p' at the dominant frequencies, at the same streamwise locations (i.e., at the same x) along both the cavity opening and the bottom [Figs. 13(c) and 13(d)]. For the *RC* case, $\gamma^2 \sim 1$ and $\Delta\phi \sim 0$ up to $x \sim 0.6$, indicating a strong coupling between the shear layer growth and the cavity acoustics. The coupling is modified at $x > 0.6$ due to the influence of shear layer impingement at the trailing edge, as evidenced by significant variations in $\Delta\phi$. However, the impingement flow is still synchronized with the cavity acoustics, as indicated by the consistent $\gamma^2 \sim 1$ in that region. For all cavity-panel configurations, except *DEP*2 and *TEP*, the value of γ^2 generally remains close to unity, indicating that their shear layer growth and the cavity acoustics are still synchronized. However, the elastic panels appear to modify and weaken the coupling of two processes to varying degrees, as seen in the fluctuations of $\Delta\phi$. The loss of coupling is most pronounced at $x \sim 0.13$, where the shear layer growth and the cavity acoustics tend to counteract each other, resulting in $\Delta\phi \sim \pi/2$. All these facts strongly support the notion that the chosen elastic panels inside the cavity act to weaken the original coupling observed in the *RC* case, leading to a reduction in overall cavity noise generation. A similar weakening of the coupling is observed in *TEP*, but its γ^2 remains below 0.5 across the length of the cavity, reaching its minimum at $x \sim 0.24$. As a result, the shear layer growth in *TEP* becomes much less synchronized with the cavity acoustics compared to all the cavity-panel configurations just discussed and the two processes are considered to be effectively decoupled. *TEP* generates much less noise as a consequence. A more complete decoupling of similar kind is observed in *DEP*2 in which its γ^2 consistently diminishes across the cavity length regardless of the $\Delta\phi$ values. As a result, *DEP*2 exhibits the lowest level of cavity noise compared to all other configurations.

VII. AEROACOUSTIC–STRUCTURAL INTERACTION OF PANELS

It is intriguing to observe the influence of aeroacoustically, or acoustically, induced vibratory responses of elastic panels on the modification of the coupling between developing shear layers and cavity acoustic modes in all cases. Figure 14 portrays the temporal progression of vibratory displacements w along the elastic panels as observed across all cases. Generally, each panel exhibits a continuous bending wave pattern over time; however, the specific type of panel bending wave it sustains is contingent upon the panel orientation. For vertical panels, transverse bending wave propagation predominates, whereas horizontal panels solely support standing bending waves. This distinction can be attributed to the varying pressure fluctuations exerted on the panel surfaces due to diverse types of aeroacoustical–structural interactions within each case.

Figure 15 depicts the vibratory acceleration $|\ddot{w}|$ spectra at the mid-points of the panels across various cases. In order to aid the discussions, blue, red, and green lines are used to indicate panel designs with designed natural frequencies (f_{EPd1}, f_{EPd2}, f_{EPd3}) = (0.925, 1.25, 1.375) at their third ($n = ③$) panel modes. In the *SEP*1 case, since the panel is situated near the cavity opening, it directly experiences p' which is of an aeroacoustic nature (Naseer *et al.*, 2023). This p' comprises fluctuations from the developing shear layer and incident acoustic fluctuations originating from the cavity bottom. It is intriguing to note that the resulting aeroacoustic–structural interaction, involving the shear layer impingement, its subsequent unsteady downwash, and the vibrating panel, leads to structural resonance at panel vibration modes $n = ①$, ②, ④, ⑦, ⑧, and ⑨ (Table I). This highly nonlinear interaction induces p' excitation with magnitudes and phases spreading across a broad frequency range, thereby favorably exciting multiple panel vibration modes simultaneously. All the excited panel vibration modes compete to absorb the energy of the p' excitation at their resonant frequencies, consequently leaving less flow fluctuation energy available for cavity resonance as compared to the *RC* case. It is surprising to observe that the dominant panel structural resonance occurs at the fourth ($n = ④$) vibration mode, rather than the third ($n = ③$) mode specified in the panel design. This particular structural resonance is believed to contribute to set the final frequency $f = 1.25$ for p', which is taken up by the developing shear layer and the cavity acoustic mode of the entire cavity-panel system [Fig. 9(b)]. In the *SEP*2 case, the panel located at the bottom of the cavity is subjected to p' solely due to the cavity acoustic resonant mode. As a result, the excitation of the panel is primarily of an acoustic nature (Naseer *et al.*, 2023). The cavity mode standing wave characteristics generate a p' with much narrower spectral magnitude distribution than that generated in *SEP*1 by impinging shear layer. This fact leads to the excitation of fewer panel vibration modes compared to the *SEP*1 case. Only vibration modes $n = ④$ and ⑧ are excited. The resultant acoustic–structural interaction of the entire cavity-panel system selects the dominant structural resonance at the fourth ($n = ④$) panel vibration mode, although a weak excitation at the designed third ($n = ③$) mode still persists. Similar to the *SEP*1 case, the bottom panel structural resonance determines the dominant frequencies of the developing shear layer and the cavity acoustic mode of the entire cavity-panel system.

In the *DEP*1 configuration, both panels from the *SEP*1 and *SEP*2 cases are installed (Fig. 5). It is interesting to note that the structural resonance of the panels exhibits a high degree of similarity to those observed in the individual *SEP*1 or *SEP*2 cases. The only notable distinction is that the *DEP*1 aft panel demonstrates a weaker response at the favored fourth ($n = ④$) mode but a stronger response at the designed third ($n = ③$) mode. This difference is believed to facilitate more effective absorption of p' energy within the cavity, as compared to the *SEP*1 or *SEP*2 cases. As discussed before, in the *DEP*2 case, the bottom panel design is changed to absorb the dominance of p' fluctuation at $f = 1.25$ inside the cavity as observed in *SEP*1, *SEP*2, and *DEP*1 cases. The combination of different panel designs into the cavity appears to result in a completely distinct type of aeroacoustic and acoustic–structural interactions from previous cases. Now the *DEP*2 aft panel shows structural resonance at panel vibration modes $n = ①$, ④, ⑦, and ⑨ but the bottom panel does not have any of its own vibration modes excited. It is surprising to observe that the bottom panel shows a particularly strong forced vibration response at $f = 1.375$ which does not coincide with any of vibration modes of the two panels. Such forced vibration response may disturb the fluid above the bottom panel and radiate a p' component at the same $f = 1.375$. This extra p' component is observed to propagate toward the aft panel and set it to vibrate with a response comparable to the excited $n = ④$ of the aft panel. The two panels appear to show a crosstalk to one another. A

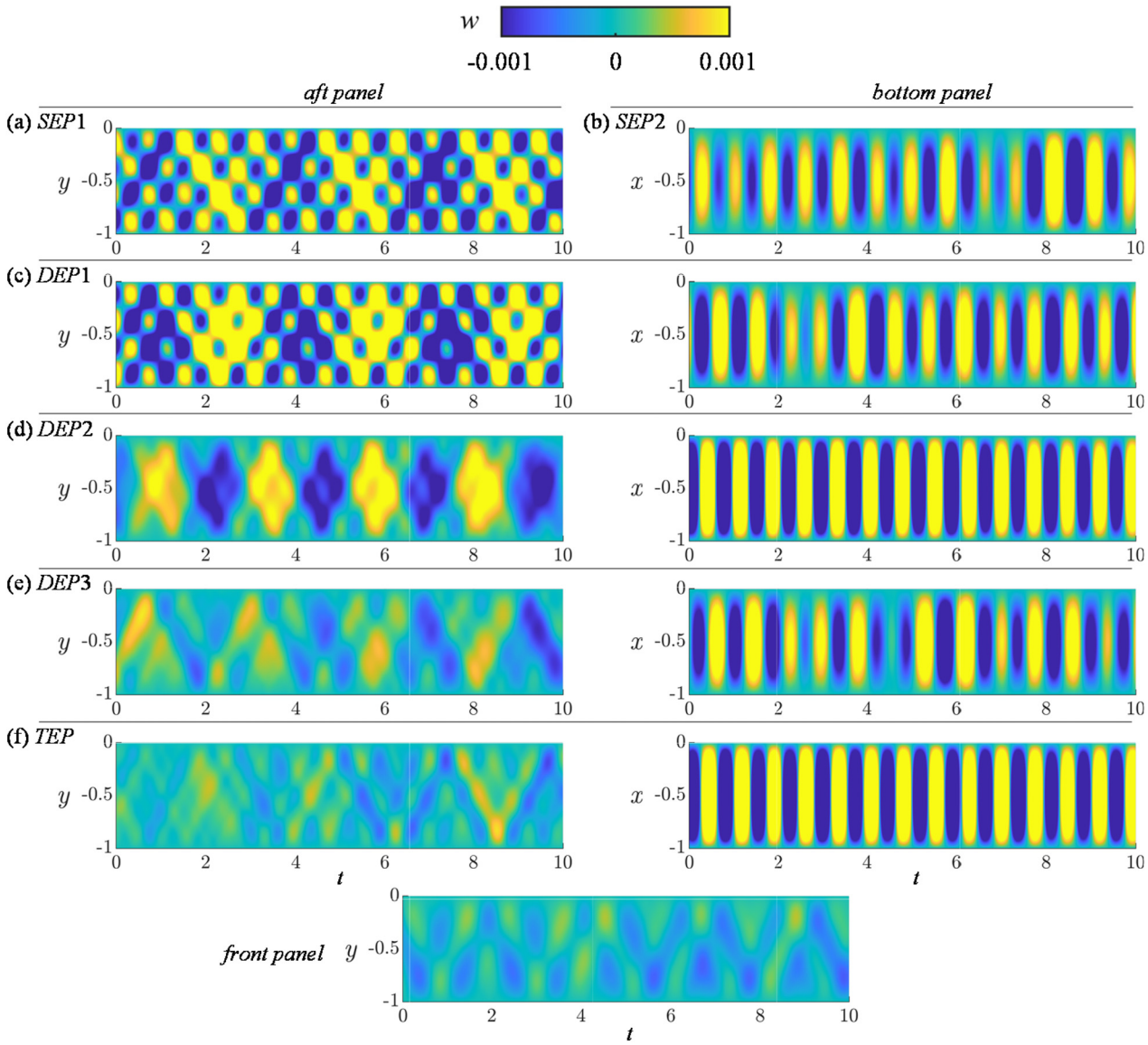

FIG. 14. Spatiotemporal panel vibratory responses. (a) *SEP*1, (b) *SEP*2, (c) *DEP*1, (d) *DEP*2, (e) *DEP*3, and (f) *TEP*.

similar phenomenon of crosstalk is also evident with bottom panel vibration for the emergence of two weak acceleration peaks at the third and ninth modes of the aft panel. This dominant frequency $f = 1.375$ is considered to an evidence for the specific cavity-panel system exhibiting synchronization between the unsteady aeroacoustics and the nonlinear dynamics of the panels. Such form of synchronization is not observed in the literature of cavity aeroacoustics. It can be considered as a form of aeroacoustic-structural resonance for the different panels in cavity configuration design. It must be noted that aeroacoustic-structural resonance does not show up in the *DEP*1 case whose both panels are the same [Fig. 15(c)].

As previously discussed, in the *DEP*2 case, the design of the bottom panel has been modified to address the dominant fluctuations of p' at $f = 1.25$ within the cavity, as observed in the *SEP*1, *SEP*2, and *DEP*1 cases. The combination of different panel designs within the cavity appears to result in a completely distinct type of aeroacoustic and acoustic–structural interactions compared to the previous cases. In the *DEP*2 configuration, the aft panel exhibits structural resonance at panel vibration modes $n = ①, ④, ⑦$, and ⑨, while the bottom panel does not have any of its own vibration modes excited. It is surprising to note that the bottom panel displays a particularly strong forced vibration response at $f = 1.375$, which does not correspond to any of the vibration modes of the two panels. This forced vibration response may disrupt the fluid above the bottom panel and generate a component of p' at the same frequency of $f = 1.375$. This additional p' component is observed to propagate toward the aft panel, causing it to

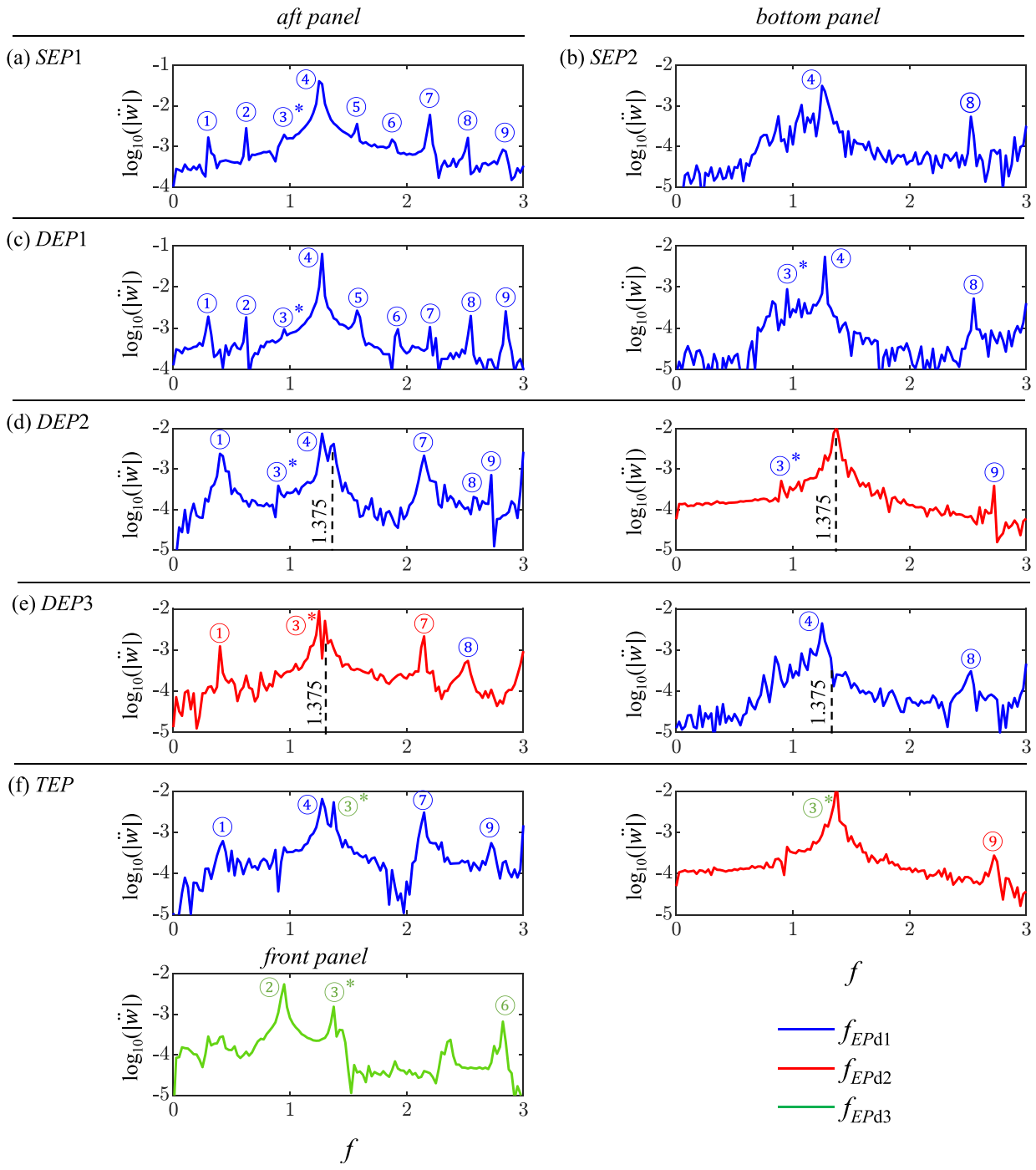

FIG. 15. Modal response of panel acceleration $|\ddot{w}|$. Spectral peaks are tagged with the modes given in Table I. The asterisk "*" means the primary designed panel natural frequencies shaded in Table I. (a) *SEP*1, (b) *SEP*2, (c) *DEP*1, (d) *DEP*2, (e) *DEP*3, and (f) *TEP*.

vibrate with a response comparable to the excited $n = 4$ mode of the aft panel. The two panels seem to exhibit a crosstalk effect, influencing the vibrations of each other. A similar phenomenon of crosstalk is also evident with the vibration of the bottom panel, resulting in the emergence of two weak acceleration peaks at the third ($n = ③$) and ninth ($n = ⑨$) modes of the aft panel. The dominant frequency of $f = 1.375$ is considered as evidence of the specific cavity-panel system *DEP*2 exhibiting synchronization between the unsteady aeroacoustics

and the nonlinear dynamics of the panels. Such a form of synchronization has not been observed in the existing literature on cavity aeroacoustics. It can be regarded as a manifestation of aeroacoustic-structural resonance in the cavity configuration design with different panels. It is important to note that aeroacoustic-structural resonance is not observed in the *DEP*1 case, where both panels are identical [Fig. 15(c)]. In the *DEP*3 case, the two panels exhibit similar vibratory responses as observed in the *DEP*2 case, albeit with their positions swapped. Although aeroacoustic-structural resonance is still present, its impact is not as pronounced as in the *DEP*2 case. The bottom panel demonstrates high vibration responses at $n = ④$ and ⑧ modes, while the aft panel exhibits significant vibration responses at $n = ①$, ③, and ⑦ [Fig. 15(d)]. Additionally, there is crosstalk occurring at the frequency corresponding to the $n = ⑧$ mode of the bottom panel. However, the magnitudes of the responses of both panels are generally weaker compared to those in the *DEP*2 case, indicating a reduced energy absorption of p' within the cavity. In the *TEP* case, a front panel is incorporated into the *DEP*2 configuration. This panel is purposefully designed to absorb the observed aeroacoustic-structural resonance at $f = 1.375$ by resonating at its own third ($n = ③$) mode. While the front panel exhibits substantial responses at its $n = ②$, ③, and ⑥ modes, its inclusion does not significantly modify the vibratory responses of the aft and bottom panels. These panels continue to display more or less the same levels of vibratory responses as in the *DEP*2 case [Fig. 15(e)], suggesting a similar ability to absorb energy from p' within the cavity.

Figure 15 clearly show that the panels in all cases are capable of entering different structural resonance at various panel vibration modes depicted in Table I. The first and third columns in Fig. 16 display the distributions of the panel acceleration $\ddot{w}$ spectra along the length of the panels in all cases. Clearly, whenever a panel is oriented vertically (i.e., the aft and front panels), all the panel resonant frequencies identified in Fig. 15 develop into their corresponding vibration mode shapes fully along the panel. The emergence of complete mode shapes provides further support for resonant responses of the panels. However, the vibratory responses of all bottom panels exhibit different behaviors. In every case, no full vibration mode shape is observed along the bottom panel, even when the frequencies of the vibratory responses match the natural frequencies depicted in Table I. Instead, the entire bottom panel seems to respond to the imposed p' in a manner similar to the forced vibration of the first mode. The particular forced vibration behavior is likely due to the specific type of acoustic–panel interaction that is driven by the cavity acoustic mode at the bottom of the cavity. The standing wave of the cavity acoustic mode may expose an acoustic p' excitation whose phase is constant along the length of the bottom panel. The constant excitation phase may not favor the development of spatial vibratory responses into their full mode shapes. On the contrary, all the vertical panels are excited by aeroacoustic p' excitation with distributed phases over a wide range of frequencies, resulting from shear layer impingement and its downwash, which favors the simultaneous development of all mode shapes fully along the bottom panel. The different characteristics of p' excitation phases on the vertical and bottom panels are believed to be responsible for the emergence of their different sustained bending wave patterns in Fig. 14.

Furthermore, it could be argued that while a panel absorbs p' energy inside the cavity through its different resonant vibration modes, the resonant vibratory accelerations may generate additional p' components, which may eventually contribute to the cavity noise radiation in the far-field location p_f. To address this concern, the coherence between the noise radiation at p_f and the p' acting on the panel surface is calculated using the similar procedure as discussed in Sec. VI, and its variation across each panel is determined (the second and fourth columns in Fig. 16). A careful comparison of the spectral distributions of the coherence and vibration acceleration reveals that not all the resonant panel vibration responses contribute to the eventual cavity noise radiation. Some resonant responses show a very high level of coherence ($\gamma^2 \to 1$) with noise radiation (marked with red double arrows), while others show an extremely low coherence ($\gamma^2 \to 0$) (marked with black double arrows) (Fig. 16). It is interesting to note that in the *DEP*2 and *TEP* cases, almost all of their strong panel acceleration peaks do not contribute to the eventual cavity noise radiation due to their almost zero coherence. There are mild contributions from a few peaks, but their panel accelerations are several orders of magnitude weaker than the strong peaks. Therefore, most panel responses in the *DEP*2 and *TEP* cases essentially act to absorb p' energy in the cavity-panel system only and do not contribute to the far-field noise radiation. This observation not only explains the root cause of the exceptionally low level of cavity noise radiation in these two cases but also further substantiates the possibility of effectively suppressing cavity noise radiation through the aeroacoustic–structural resonance of two properly designed panel inside the cavity.

VIII. IMPLEMENTATION GUIDELINES OF THE PROPOSED NOISE REDUCTION CONCEPT

To concisely explain the proposed cavity noise suppression concept that leverages multiple elastic panels, implementation guidelines are outlined here based on the insights gained from the present and our previous (Naseer *et al.*, 2023) studies.

(a) Thorough analysis of rigid cavity flow characteristics
- The analysis aims to identify all locations on the cavity walls that support the flow processes responsible for cavity aeroacoustic feedback. These locations are the ideal positions for the placement of elastic panels to modify the identified flow processes. It is crucial to determine the dominant frequencies of the flow processes, as they will be the defining physical parameters for the structural designs of the panels.

(b) Specification of elastic panel
- Each elastic panel is expected to extract the flow fluctuation energy of a particular aeroacoustic feedback process identified in (b) through its resonant vibration excited by the flow and acoustic excitation naturally occurring in the cavity flow. To achieve this, the fluid-loaded natural frequency of an elastic panel is selected as the working frequency, which must match an identified flow frequency.
- The setting of the working frequency of a panel is guided by Eq. (1). The length, thickness, tension, and material properties are considered as the adjustable parameters for the working frequency. The panel length is typically constrained by the flow problem. The panel tension is usually set to a small value for ease of its application in practical applications. The panel thickness and material properties are the more convenient parameters for adjustment.

(c) Setting of cavity-panel configurations

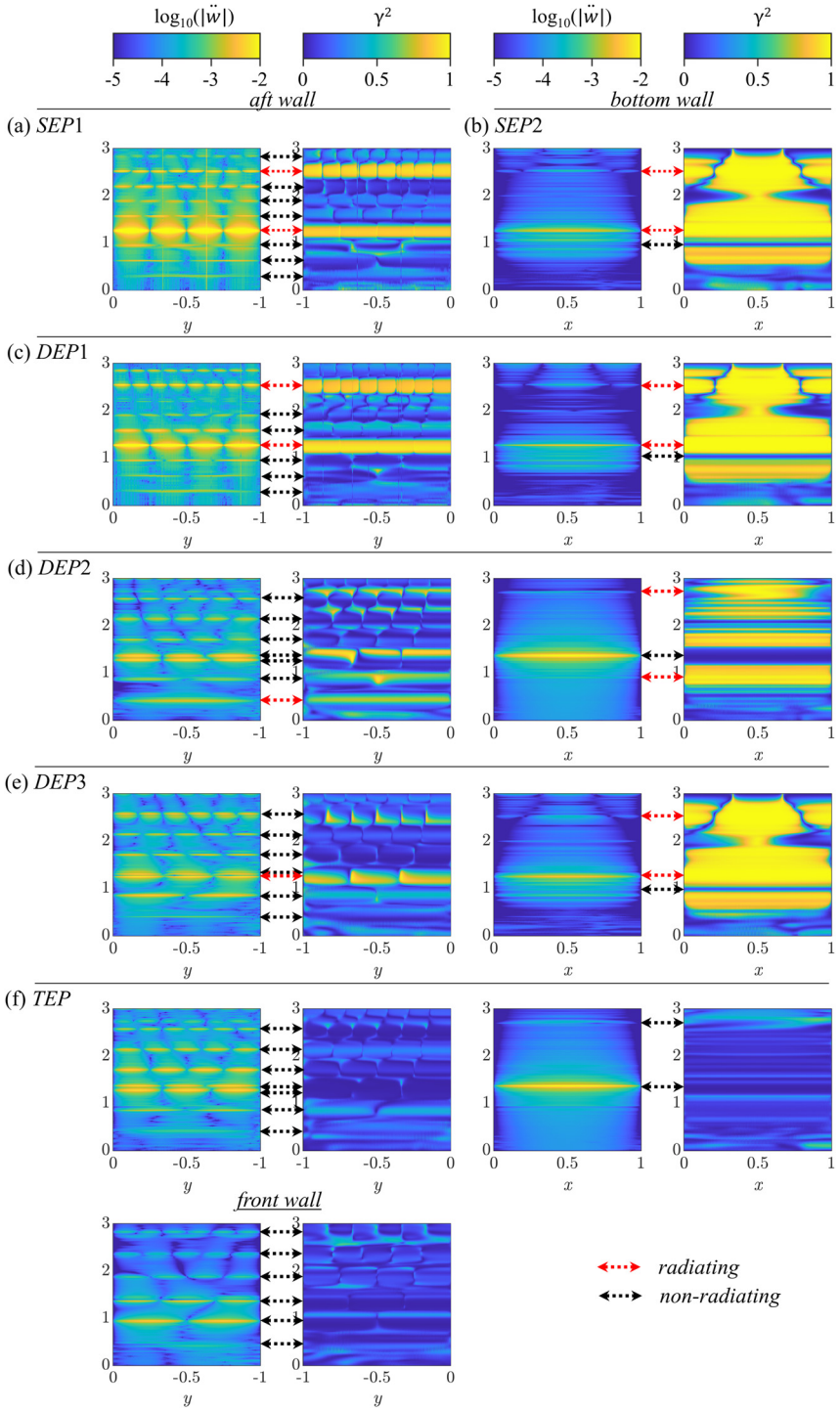

FIG. 16. First column and third column: variation of FFT transformed of aft and bottom panel acceleration; second and fourth column: spectra of magnitude-squared coherence γ^2 between the acoustic signal at p_f and pressure signals along the respective panel surface. (a) *SEP*1, (b) *SEP*2, (c) *DEP*1, (d) *DEP*2, (e) *DEP*3, and (f) *TEP*.

- It begins with the modification using a single elastic panel. The setting of this panel may proceed in the same manner as reported in Sec. III. Typically, the modification targets the more energetic aeroacoustic feedback process, followed by the processes with weaker energy content. Special attention must be paid to any shift in the dominant frequencies of the modified flow.
- If stronger cavity noise suppression is desired, configurations with multiple elastic panels can be explored. However, one must be cautious that the new elastic panels

may be designed based on the dominant frequencies of the modified flow, rather than the original ones with the rigid cavity flow. The configuration can proceed in a similar manner as reported in Sec. IV.

IX. CONCLUSIONS

In this paper, we have meticulously explored a unique passive approach for suppressing the deep cavity noise, employing a distributed surface compliance mechanism via strategic designs and arrangements of multiple elastic panels. The study involves a detailed numerical analysis on a two-dimensional flow past a deep cavity characterized by a length-to-depth ratio of 0.4, exposed to the low Mach number flow ($M = 0.09$) and a Reynolds number $Re = 4 \times 10^4$ based on cavity length. The focus of the study delves into the complex dynamics of cavity flows, scrutinizing the intricacies of noise generation processes influenced by the placement of single, double, and triple panels at various cavity wall locations. Our initial analysis encompasses both a rigid cavity and five distinct cavity-panel configurations with a single panel that provide critical insights into flow characteristics. These findings inform the development of five novel cavity-panel arrangements, featuring double and triple panel configurations, aimed at accentuating the maximum cavity noise reduction. The design rationale for these multiple panel configurations is grounded in two fundamental observations: the predominance of shear layer fluctuations near the cavity aft wall adjacent to the cavity trailing edge, and the dominant acoustic modes operating at the cavity bottom. By meticulously targeting these pivotal aspects of the cavity aeroacoustic mechanism with strategically designed elastic panels, the proposed approach is envisaged to significantly influence, and thereby mitigate, the noise generation processes.

In assessing the efficacy of the novel cavity-panel configurations for noise suppression, we solve the cavity aeroacoustics by means of Direct Aeroacoustic Simulation (DAS) coupled with panel structural dynamics solver in monolithic fashion. Among these, a double panel configuration, namely the *DEP*2 case, emerges as the most effective in mitigating cavity tonal noise by almost 15 dB. This particular arrangement strategically employs aft and bottom wall panels, where fluid-loaded natural frequencies are precisely tuned to target specific dominant flow frequencies. The success of *DEP*2 case can be attributed to its adept harnessing of aeroacoustic–structural interactions of panels for effective suppressing the flow and acoustic fluctuation energy of the cavity. Other double panel configurations also demonstrate a certain level of noise reduction but their effectiveness varies. Interestingly, the triple panel configuration *TEP*, which builds upon the same principles as the *DEP*2 setup, does not yield extra noise reduction benefits of a third panel on the cavity front wall. This outcome underscores the complexity of aeroacoustic interactions and the challenge of optimizing panel arrangements for maximal noise suppression.

Extensive analyses of numerical results reveal that employing strategically designed elastic panels in various configurations can alter the aeroacoustic feedback mechanisms responsible for fluid-resonant oscillations in deep cavities in different fashion. A notable observation is the high contrast in the energy transfer dynamics between the growing shear layer and cavity acoustic modes exhibited in the baseline rigid cavity case (*RC*) and various cavity-panel configurations. In the *RC* case, the energy of flow fluctuation due to shear layer impingement at cavity trailing edge is efficiently channeled to generate a strong cavity acoustic mode. However, this dynamics behaves significantly different in the cavity-panel configurations, where the interaction of the shear layer with the cavity aft wall only leads to a weak cavity acoustic mode. The detailed study of the spectral and phase information of shear layer flow and cavity acoustic mode fluctuations in the *DEP*2 case shows a distinct deviation from the *RC* case. In *DEP2* case, the shear layer fluctuation and cavity acoustic mode operate at different frequencies and are completely out-of-phase, exhibiting a total distortion in their coherence. This indicates that the critical locked-on condition, defined in the *RC* case by the criteria of $f_1 = f_{\text{shear layer}} = f_{\text{acoustic mode}}$, $\gamma^2(f_1) \sim 1$, and $\Delta\phi(f_1) \sim 0$, is significantly disrupted with the multiple elastic panels introduced. Moreover, the analysis of frequency modulation along the cavity front and aft walls elucidates that the original *RC* dominant frequency is split into the multiple cavity acoustic modes in the cavity-panel configuration. Therefore, this constitutes a re-distribution of flow/acoustic fluctuation energy across multiple cavity modes, which may interact with each other with different relative phases and play a pivotal role in modulating the ultimate cavity noise radiation.

The aeroacoustic–structural interaction of panels within deep cavities has provided a good insight into effective noise reduction mechanisms. Our study reveals that the flow-induced elastic panels significantly influence the coupling between developing shear layers and cavity acoustic modes. Each panel dictates its specific bending wave pattern with respect to its orientation. Vertical panels predominantly exhibit transverse bending wave propagation while horizontal panels support standing bending waves. Such kind of preference is attributed to different aeroacoustic–structural interactions marked by distinct pressure fluctuations. The panels in structural resonance interact with the flow and acoustic fluctuation in unique ways and lead to significant alterations in cavity noise generation characteristics. Notably, in *DEP*2 and *TEP* cases, the panels do not contribute to far-field noise radiation despite their strong vibratory responses, indicating their primary role in absorbing flow fluctuation energy within the cavity-panel systems. The observation of this new phenomenon of aeroacoustic-structural resonance, in multiple panel configurations highlights the potential of the proposed passive approach for effectively suppressing cavity noise radiation.

Another unique aspect of the proposed approach lies in the minimal distortion of the original flow characteristics. It is achieved by maintaining the resonant vibratory panel displacement smaller than the typical cavity dimensions and utilizing the reactive nature of structural resonance for energy absorption rather than traditional dissipative methods. More important to note is that the flow dynamic consequences of the proposed passive approach gives an unintended advantage of remarkable drag reduction (as much as 15% in *DEP*2 case) providing crucial attractiveness of implementing the proposed noise suppression technique in engineering applications.

Last but not the least, the present study contributes a novel, effective, yet minimally invasive approach to cavity noise suppression. The physical insights gained from the study are expected to guide future research and development in noise control strategies with similar advantages, especially in engineering applications where the flow-induced cavity noise is a critical concern.

ACKNOWLEDGMENTS

The authors gratefully acknowledge the support from the Research Grants Council of the Government of Hong Kong Special

Administrative Region under Grant No. 15208520. The first author is grateful to the stipend support to his study tenable at Department of Mechanical Engineering, The Hong Kong Polytechnic University.

AUTHOR DECLARATIONS

Conflict of Interest

The authors have no conflicts to disclose.

Author Contributions

Muhammad Rehan Naseer: Data curation (equal); Formal analysis (equal); Investigation (equal); Software (equal); Validation (equal); Visualization (equal); Writing – original draft (equal). **Irsalan Arif:** Data curation (equal); Investigation (equal); Methodology (equal); Software (equal); Writing – review & editing (equal). **Randolph C. K. Leung:** Conceptualization (equal); Formal analysis (equal); Funding acquisition (equal); Project administration (equal); Resources (equal); Software (equal); Supervision (equal); Writing – review & editing (equal). **Ali Abdullah:** Investigation (equal); Software (equal); Validation (equal); Visualization (equal).

DATA AVAILABILITY

The data that support the findings of this study are available from the corresponding author upon reasonable request.

REFERENCES

Abdelmwgoud, M. and Mohany, A., "Control of the self-sustained shear layer oscillations over rectangular cavities using high-frequency vortex generators," Phys. Fluids **33**(4), 045115 (2021).
Arif, I., Lam, G. C. Y., Wu, D., and Leung, R. C. K., "Passive airfoil tonal noise reduction by localized flow-induced vibration of an elastic panel," Aerosp. Sci. Technol. **107**, 106319 (2020).
Arif, I., Lam, G. C. Y., Leung, R. C. K., and Naseer, M. R., "Distributed surface compliance for airfoil tonal noise reduction at various loading conditions," Phys. Fluids **34**(4), 046113 (2022).
Arif, I., Naseer, M. R., Leung, R. C. K., and Salamat, S., "Control of acoustic scattering of trailing edge flow by distributed compliance," Phys. Fluids **35**(10), 106115 (2023).
Arya, N. and De, A., "Effect of vortex and entropy sources in sound generation for compressible cavity flow," Phys. Fluids **33**(4), 046107 (2021).
Bacci, D. and Saddington, A. J., "Hilbert–Huang spectral analysis of cavity flows incorporating fluidic spoilers," AIAA J. **61**(1), 271–284 (2022).
Bacci, D. and Saddington, A. J., "Influence of door gap on aeroacoustics and structural response of a cavity," AIAA J. **62**(3), 1021–1036 (2023).
Bruggeman, J. C., Hirschberg, A., van Dongen, M. E. H., Wijnands, A. P. J., and Gorter, J., "Flow induced pulsations in gas transport systems: analysis of the influence of closed side branches," J. Fluids Eng. **111**(4), 484–491 (1989).
Bruggeman, J. C., Hirschberg, A., van Dongen, M. E. H., Wijnands, A. P. J., and Gorter, J., "Self-sustained aero-acoustic pulsations in gas transport systems: Experimental study of the influence of closed side branches," J. Sound Vib. **150**(3), 371–393 (1991).
Cattafesta III, L. N., Song, Q., Williams, D. R., Rowley, C. W., and Alvi, F. S., "Active control of flow-induced cavity oscillations," Prog. Aerosp. Sci. **44**(7–8), 479–502 (2008).
Covert, E. E., "An approximate calculation of the onset velocity of cavity oscillations," AIAA J. **8**(12), 2189–2194 (1970).
East, L. F., "Aerodynamically induced resonance in rectangular cavities," J. Sound Vib. **3**(3), 277–287 (1966).
El Hassan, M., Keirsbulck, L., and Labraga, L., "Aero-acoustic coupling Inside large deep cavities at low-subsonic speeds," J. Fluids Eng. **131**(1), 011204 (2008).
Fan, H. K. H., Leung, R. C. K., Lam, G. C. Y., Aurégan, Y., and Dai, X., "Numerical coupling strategy for resolving in-duct elastic panel aeroacoustic/structural interaction," AIAA J. **56**(12), 5033–5040 (2018).
Forestier, N., Jacquin, L., and Geffroy, P., "The mixing layer over a deep cavity at high-subsonic speed," J. Fluid Mech. **475**, 101–145 (2003).
Gharib, M. and Roshko, A., "The effect of flow oscillations on cavity drag," J. Fluid Mech. **177**, 501–530 (1987).
Heller, H. H. and Bliss, D. B., "Aerodynamically induced pressure oscillations in cavities—Physical mechanisms and suppression concepts," Technical Report No. AFFDL-TR-74-133 (AF Flight Dynamics Laboratory, Wright-Patterson AFB, 1975).
He, Y., Thompson, D., and Hu, Z., "Aerodynamic noise from a high-speed train bogie with complex geometry under a leading car," J. Wind Eng. Ind. Aerodyn. **244**, 105617 (2024).
Ho, Y. W. and Kim, J. W., "A wall-resolved large-eddy simulation of deep cavity flow in acoustic resonance," J. Fluid Mech. **917**, A17 (2021).
Howe, M. S., "Vortex sound," in *Theory of Vortex Sound*, Cambridge Texts in Applied Mathematics (Cambridge University Press, Cambridge, 2002), pp. 114–135.
Howe, M. S., *Theory of Vortex Sound* (Cambridge University Press, 2003).
Kook, H., Mongeau, L., Brown, D. V., and Zorea, S. I., "Analysis of the interior pressure oscillations induced by flow over vehicle openings," Noise Control Eng. J. **45**, 223–234 (1997).
Lam, G. C. Y., Leung, R. C. K., Seid, K. H., and Tang, S. K., "Validation of CE/SE scheme in low Mach number direct aeroacoustic simulation," Int. J. Nonlinear Sci. Numer. Simul. **15**(2), 157–169 (2014).
Lam, G. C. Y., Leung, R. C. K., and Tang, S. K., "Aeroacoustics of duct junction flows merging at different angles," J. Sound Vib. **333**(18), 4187–4202 (2014).
Larchevêque, L., Sagaut, P., Mary, I., Labbé, O., and Comte, P., "Large-eddy simulation of a compressible flow past a deep cavity," Phys. Fluids **15**(1), 193–210 (2003).
Lee, B. H. K., "Effect of a perturbed shear layer on cavity resonance," J. Aircr. **47**(1), 343–345 (2010).
Li, B., Ye, C.-C., Wan, Z.-H., Liu, N.-S., Sun, D.-J., and Lu, X.-Y., "Noise control of subsonic flow past open cavities based on porous floors," Phys. Fluids **32**(12), 125101 (2020).
Liu, Q. and Gaitonde, D., "Acoustic response of turbulent cavity flow using resolvent analysis," Phys. Fluids **33**(5), 056102 (2021).
Liu, Q. and Gómez, F., "Role of trailing-edge geometry in open cavity flow control," AIAA J. **57**(2), 876–878 (2019).
Liu, Y., Chen, B., Shi, Y., and Rong, A., "Visualization of pressure fluctuation characteristics of weapon bay on unmanned aerial vehicle using delayed detached eddy simulation," J. Vis. **27**(1), 75–87 (2024).
Liu, Y., Liu, P., Guo, H., Hu, T., and Zhang, J., "Investigation of the dominant Rossiter modal tones at the locked-on state," J. Sound Vib. **556**, 117741 (2023).
Maury, C., Bravo, T., and Mazzoni, D., "The use of microperforations to attenuate the cavity pressure fluctuations induced by a low-speed flow," J. Sound Vib. **439**, 1–16 (2019).
Mourão Bento, H. F., VanDercreek, C. P., Avallone, F., Ragni, D., and Snellen, M., "Lattice Boltzmann very large eddy simulations of a turbulent flow over covered and uncovered cavities," Phys. Fluids **34**(10), 105120 (2022).
Naseer, M. R., Arif, I., Lam, G. C. Y., and Leung, R. C. K., "Effect of flow-induced surface vibration on deep cavity aeroacoustics," AIAA Paper No. 2022-2958, 2022.
Naseer, M. R., Arif, I., Leung, R. C. K., and Lam, G. C. Y., "Suppression of deep cavity aeroacoustics at low Mach number by localized surface compliance," Phys. Fluids **35**(5), 056115 (2023).
Plentovich, E. B., Stallings, R. L., and Tracy, Jr., M. B., "Experimental cavity pressure measurements at subsonic and transonic speeds," Report No. NAS 1.60:3358 (NASA, 1993).
Powell, A., "Theory of vortex sound," J. Acoust. Soc. Am **36**, 177–195 (1964).
Rebholz, P. S., Krebietke, S., Abhari, R. S., and Kalfas, A. I., "Turbine aerodynamic low-frequency oscillation and noise reduction using partial shrouds," J. Propul. Power **32**(5), 1067–1076 (2016).
Rockwell, D. and Naudascher, E., "Review—Self-sustaining oscillations of flow past cavities," J. Fluids Eng. **100**(2), 152–165 (1978).

Rossiter, J. E., "Wind-tunnel experiments on the flow over rectangular cavities at subsonic and transonic speeds," Report No. 3438 (Aeronautical Research Council, 1964).
Saddington, A. J., Thangamani, V., and Knowles, K., "Comparison of passive flow control methods for a cavity in transonic flow," J. Aircraft **53**(5), 1439–1447 (2016).
Talotte, C., "Aerodynamic noise: A critical survey," J. Sound Vib. **231**(3), 549–562 (2000).
Wang, P., Jia, S., He, Z., He, C., Sung, H. J., and Liu, Y., "Flow–acoustic resonance mechanism in tandem deep cavities coupled with acoustic eigenmodes in turbulent shear layers," J. Fluid Mech. **984**, A19 (2024).
Yang, Y., Rockwell, D., Cody, K. L.-F., and Pollack, M., "Generation of tones due to flow past a deep cavity: Effect of streamwise length," J. Fluids Struct. **25**(2), 364–388 (2009).
Yamouni, S., Sipp, D., and Jacquin, L., "Interaction between feedback aeroacoustic and acoustic resonance mechanisms in a cavity flow: A global stability analysis," J. Fluid Mech. **717**, 134–165 (2013).
Yokoyama, H., Odawara, H., and Iida, A., "Effects of freestream turbulence on cavity tone and sound source," Int. J. Aerosp. Eng. **2016**, 7347106.
Yokoyama, H., Tanimoto, I., and Iida, A., "Experimental tests and aeroacoustic simulations of the control of cavity tone by plasma actuators," Appl. Sci. **7**(8), 790 (2017).
Yokoyama, H., Otsuka, K., Otake, K., Nishikawara, M., and Yanada, H., "Control of cavity flow with acoustic radiation by an intermittently driven plasma actuator," Phys. Fluids **32**(10), 106104 (2020).
Ziada, S., Oengören, A., and Vogel, A., "Acoustic resonance in the inlet scroll of a turbo-compressor," J. Fluids Struct. **16**(3), 361–373 (2002).
Ziada, S., "Flow-excited acoustic resonance in industry," J. Pressure Vessel Technol. **132**(1), 015001 (2010).
Ziada, S. and Bühlmann, E. T., "Self-excited resonances of two side-branches in close proximity," J. Fluids Struct. **6**(5), 583–601 (1992).